GeoExpert ag

swiss*nuclear*: PEGASOS Refinement Project:
SP2 – Ground Motion Characterization

Contract no. PMT-VT-1032

Seismic Shear Wave Velocity Determination and Hybrid Seismic Survey at the SED-Station ACB (Klingnau AG)

Date of Field Data Acquisition 3rd March 2009

Report

Client

swiss*nuclear*
Project PRP
Frohburgstrasse 17
4601 Olten

Contractor

GeoExpert ag
Seismic Prospecting
Ifangstrasse 12b
P.O. Box 451
8603 Schwerzenbach

8603 Schwerzenbach, 13th May 2009

INDEX

1 INTRODUCTION

1.1 Survey objectives

The seismic survey's main task is to provide information about the distribution function of the shear wave velocities in the depth interval of the uppermost 30 m along a 100 m long seismic profile.

Additionally, the following objectives are to be met:

- the mapping of the topography of the rock face, i.e. the thickness of the Quaternary deposits;
- the determination of the thickness of the weathered zone and its degree of decompaction at the bedrock surface;
- a general view of geological structures.

1.2 The choice of the appropriate surveying methods

Several methods are available for deriving the s-wave velocity distribution in the subsurface at any given position:

- in-situ measurement by down-hole or crosshole seismic surveying;
- shear-wave refraction tomography profiling;
- dispersion analysis of surface waves (MASW; **M**ultiple channel **A**nalysis of **S**urface **W**aves)

The surveys are to be carried out at, or as close as possible near some 20 SED earth quake monitoring stations in Switzerland. Ideally, the surveys are to be conducted on two orthogonal profiles in order to derive at their point of intersection a robust 1D s-wave velocity distribution function by correlation. To this end, the methods of MASW and shear-wave refraction tomography profiling are to be combined.

The results are to include the following fundamental parameters $v_{s,5}$, $v_{s,10}$, $v_{s,20}$, $v_{s,30}$, $v_{s,40}$, $v_{s,50}$, $v_{s,100}$ are to be calculated, also an error estimation of all values.

The data acquired for the MASW method are to be subjected to complementary **p-wave hybrid seismic data processing** in order to image the geological structures.

2 FIELD DATA ACQUISITION PARTICULARS

2.1 Time Schedule

Date	*Time*	*Activities / remarks*
03.03.2009	1030	arrival from Schwerzenbach
	1030 - 1045	site reconnaissance
	1045 - 1200	lay-out of recording spread profile 1 p-wave
	1310 - 1350	compressional wave data recording profile 1
	1430	departure from site
05.03.2009	1000	arrival from Schwerzenbach
	1000 - 1120	lay-out of recording spread profile 2 s- and p-wave
	1130 - 1230	compressional wave data recording profile 2
	1310 - 1410	shear wave data recording profile 2
	1450 - 1530	lay-out of recording spread profile 1 p-wave
	1530 - 1615	retrieval of the recording spread
	1615	departure from site

2.2 Summary of Data Acquisition Parameters

Compressional Wave Data Acquisition

# of active channels	96
geophone type	4.5 Hz natural frequency, vertical velocimeter
receiver station spacing	1.0 m
# of geophones/station	1
source point spacing	2.0 m to 3.0 m
source type	vertical hammer (6 kg) striking on a horizontal metal plate
sampling rate	500 µs
recording time	2048 ms
field filters	0.5 Hz LC, anti-alias
# of field records	48 (line 09SN_01ACB-P1) and 49 (line 09SN_01ACB-P2)

Shear Wave Data Acquisition

# of active channels	48
geophone type	10 Hz natural frequency, horizontal velocimeter
receiver station spacing	2.0 m
# of geophones/station	1
source point spacing	4.0 m to 6.0 m
source type	horizontal hammer (6 kg) striking horizontally at a metal-plated wooden beam anchored to the ground by means of 20 cm long spikes
sampling rate	500 µs
recording time	512 ms
field filters	2 Hz LC, anti-alias
# of field records	44 at 22 positions (line 09SN_01ACB-S1) and 38 (line 09SN_01ACB-S2)

Fig. 2.1: S-wave data acquisition at profile 09SN_01ACB-S2.

2.3 Composition of Seismic Field Crew

Personnel

Jochen Fiseli	Dipl.-Geolog, University of Freiburg I. Br., party chief
Dieter Martin	Dipl.-Geolog, University of Freiburg I. Br., party chief
Kieron Lynch	assistant, spread lay-out and activation of seismic source
Fabian Isler	assistant, spread lay-out and activation of seismic source

Equipment

96	vertical geophones 4.5 Hz
48	horizontal geophones 12 Hz
6	seismic cables
1	seismic acquisition system Summit Compact, 96 channels
1	laptop computer for data acquisition
3	walkie-talkies
1	hammer 6 kg
1	steel plate
1	metal-plated wooden beam
1	van (FIAT Ducato 4x4)

2.4 Location

The seismic monitoring station ACB (Klingnau AG) is situated on the top of a Jurassic sediment ridge in northern Switzerland, canton of Aargau, immediate adjacent to Quaternary fluvioglacial deposits (Terrassenschotter).

Fig. 2.2: The red cross marked seismic monitoring station ACB (Klingnau AG) is located in Aargau's Jurassic sediments (Dogger). (map: geodata @ swisstopo).

2.5 Recording Conditions and Line Setup

Drizzle and low temperatures prevailed throughout the field data recording period with little of snow covering the soil.

In general, the data quality obtained at ACB is to be rated as fair.

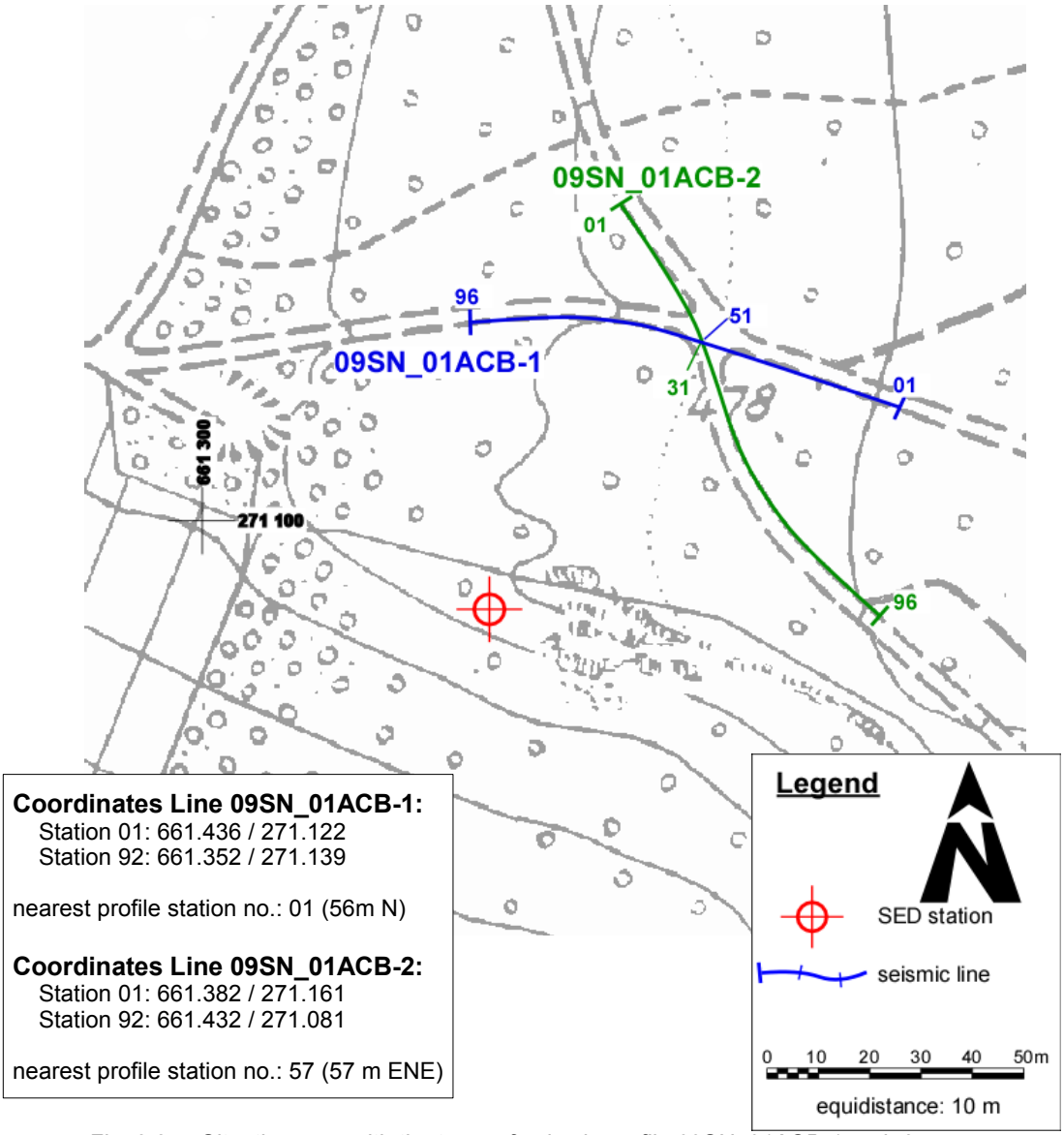

Fig. 2.3: Situation map with the trace of seismic profile 09SN_01ACB-1 and -2. (background map: © AGIS canton of Aargau.)

3 SEISMIC DATA PROCESSING AND IMAGING OF THE RESULTS

3.1 General Remarks

- For the shear and compressional wave refraction seismic evaluation the package **RAYFRACT** by Intelligent Resources Ltd., Vancouver CAN, was used. The system features the technique of diving wave tomography (www.rayfract.com).
- The system **SPW** (**S**eismic **P**rocessing **W**orkshop) of Parallel Geoscience Corporation, Austin US-TX, was used for reflection seismic data processing (www.parallelgeo.com).
- Data processing of surface waves (MASW processing) was conducted with the software package **SurfSeis** V2.0 of Kansas Geological Survey in Lawrence US-KS.

A detailed description of the various surveying methods will be included in the general summary report.

3.2 Shear Wave Refraction Tomography

3.2.1 Reformatting and field geometry assignment

After reformatting the field data into the Rayfract format the field geometry is applied.

3.2.2 First break time picking

At each shot position, two seismic records were acquired in both activation directions. These two records are displayed superimposed with different colors on each other in Fig 3.2a together with the manually determined first arrival time picks.

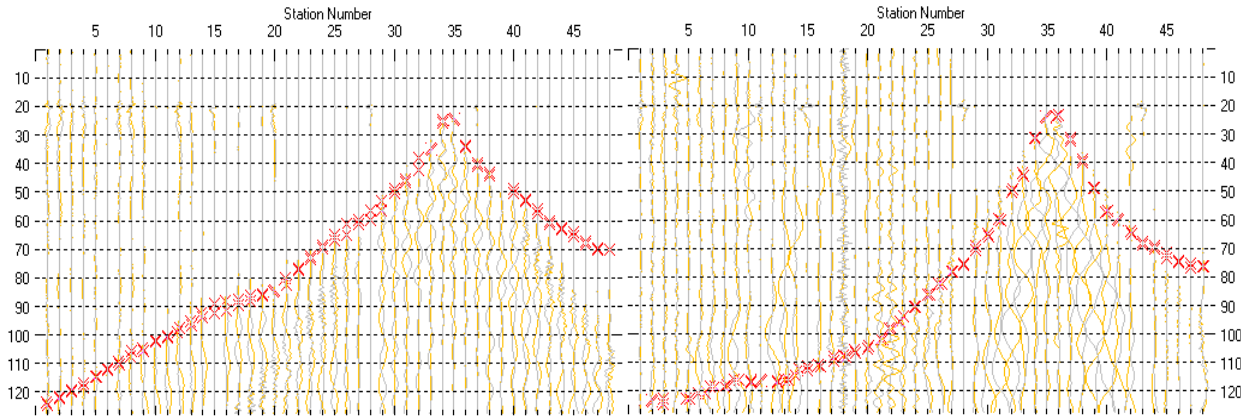

*Fig. 3.2a: High quality dual field record from line 09SN_01ACB-S1 (left) and 09SN_01ACBN-S2 (right).showing at each station the s-wave traces with opposing polarities in different colors. The manually picked s-wave refraction arrivals at each station are marked with an **x**. The station spacing is 2 m, profile station number 00 = profile meter 0; profile station number 48 = profile meter 96.*

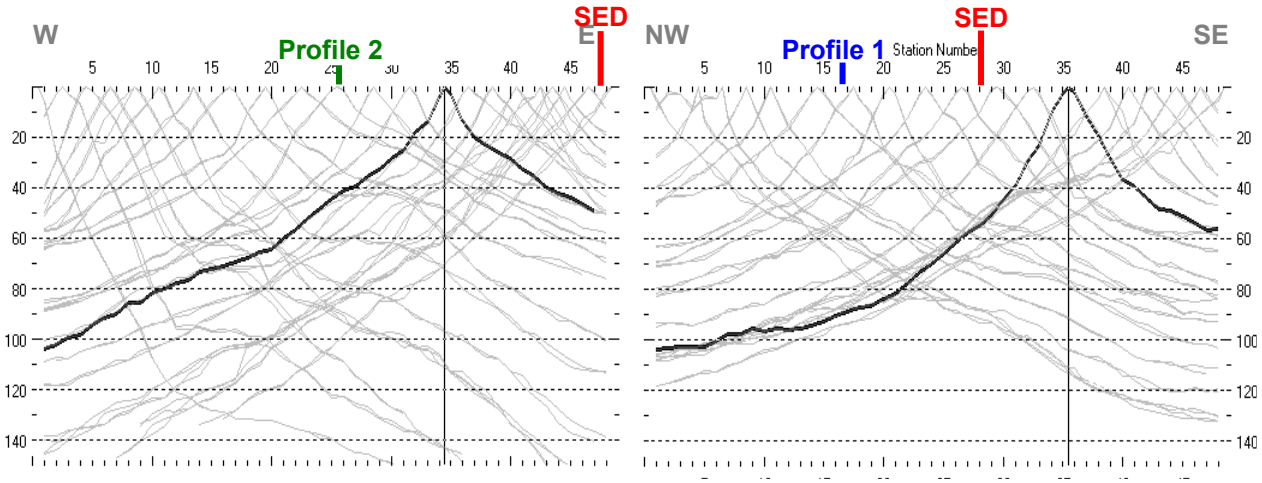

Fig. 3.2b: Curves of s-wave first break time picks from line 09SN_01ACB-S1 (left) and 09SN_01ACB-S2 (right).

3.2.3 Analytical Determination of Refraction Velocities

An initial 1D-velocity function (averaged 1D velocity-depth profiles derived by the Delta-t-V method, see Tab. 3.2a) is determined in the 3-dimensional time-offset-CMP-domain from all first break arrival time curves in the 3-dimensional time-offset-CMP-domain (see. Fig. 3.2c).

Depth [m]	Vs [m/s]
0.0	354
0.4	353
0.7	359
1.3	376
1.8	412
2.7	482
3.8	584
5.4	758
7.4	852
10.3	692
13.9	581
19.1	576
26.0	800
35.1	918
47.6	681

Depth [m]	Vs [m/s]
0.0	356
0.4	359
0.7	368
1.1	381
1.8	414
2.5	435
3.4	475
4.7	570
6.5	726
8.8	797
11.9	665
16.0	580
21.6	633
28.8	701
38.6	811
50.3	605

Tab. 3.2a: Initial 1D s-wave velocity function derived from real data from line 09SN_01ACB-S1 (mean values between profile meters 45 and 65) and from line 09SN_01ACB-S2 (mean values between profile meters 30 and 55).

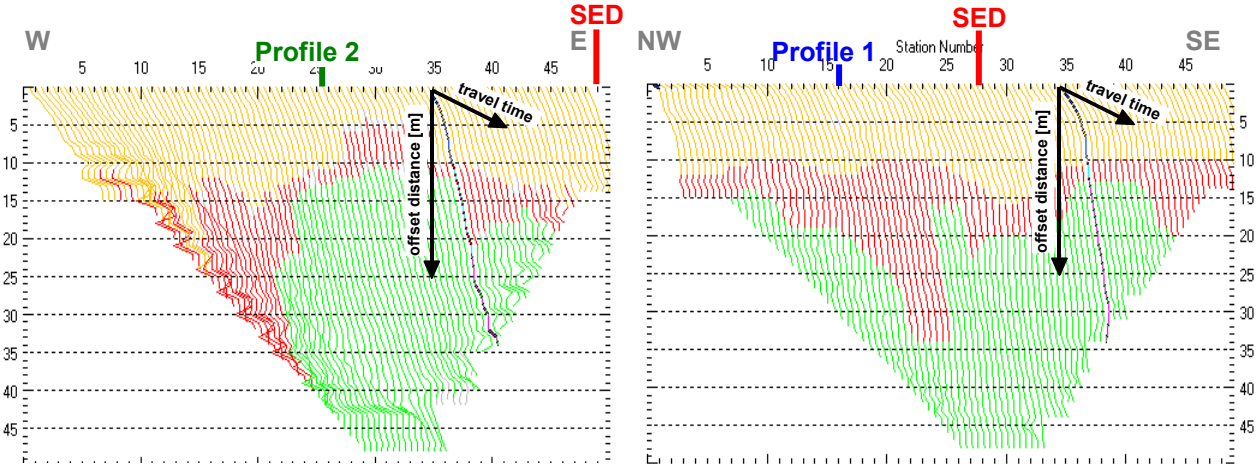

Fig. 3.2c: 3-dimensional distance-travel time diagrams from line 09SN_01ACB-S1 (left) and 09SN_01ACB-S2 (right) at the mid-points between source points and receiver stations are instrumental when using the analytical CMP derivation of the initial velocity field.
The horizontal axes are the along the CMP positions and the travel time respectively, the vertical axis denotes the offset distance between source and receiver positions. The colors represent different velocity layers. The station spacing is 2 m, profile station number 00 = profile meter 0; profile station number 48 = profile meter 96. The colors represent different velocity layers.

3.2.4 Tomographic inversion of the velocity gradient field by iterative modeling

The velocity field is iteratively refined by the subsequent Wavepath Eikonal Traveltime (WET) tomographic inversion process. The inversion results are portrayed in Fig. 3.2d as a gridded velocity contour section and in Fig. 3.2e as a ray path density section.

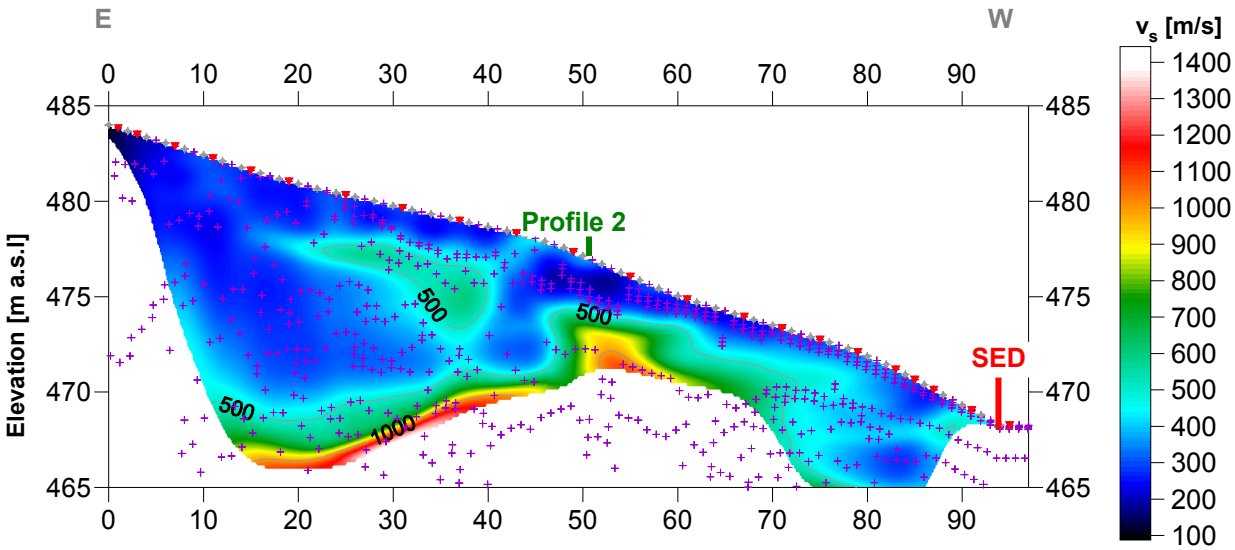

Fig. 3.2d: Shear wave velocity field of the line 09SN_01ACB-S1. Red/white colors denote solid rock, blue/black colors point to unconsolidated sediments and soil.
Vertical axis: elevation [m a.s.l]; horizontal axis: profile meter; color encoded scale: v_s [m/s]; vertical exaggeration: 2:1; gray diamonds: receiver positions; red triangles: source positions; magenta crosses: positions of determined velocity values. The station spacing is 2 m, profile meter 0 = profile station number 00, profile meter 96 = profile station number 48.

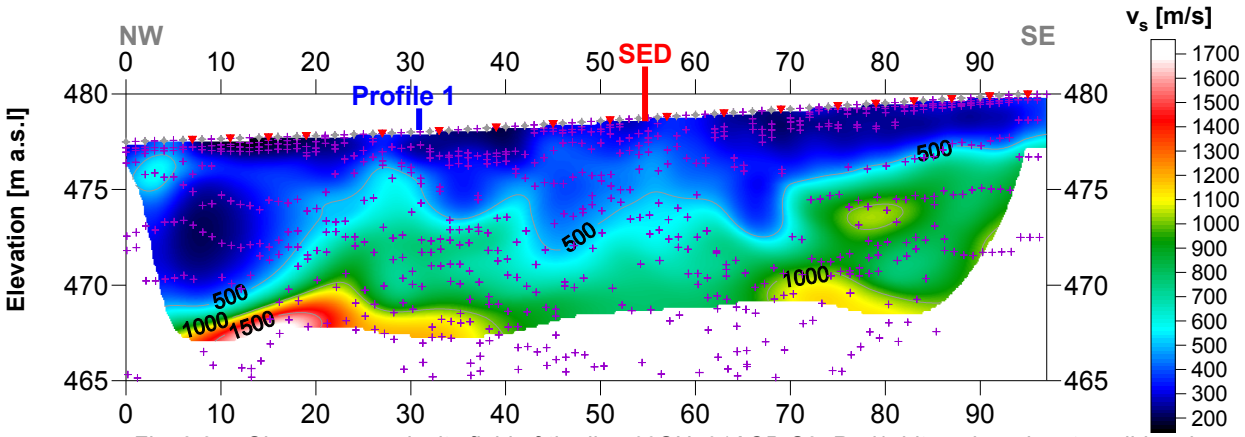

Fig. 3.2e: Shear wave velocity field of the line 09SN_01ACB-S2. Red/white colors denote solid rock, blue/black colors point to unconsolidated sediments and soil.
Vertical axis: elevation [m a.s.l]; horizontal axis: profile meter; color encoded scale: v_s [m/s]; vertical exaggeration: 2:1; gray diamonds: receiver positions; red triangles: source positions; magenta crosses: positions of determined velocity values. The station spacing is 2 m, profile meter 0 = profile station number 00, profile meter 96 = profile station number 48.

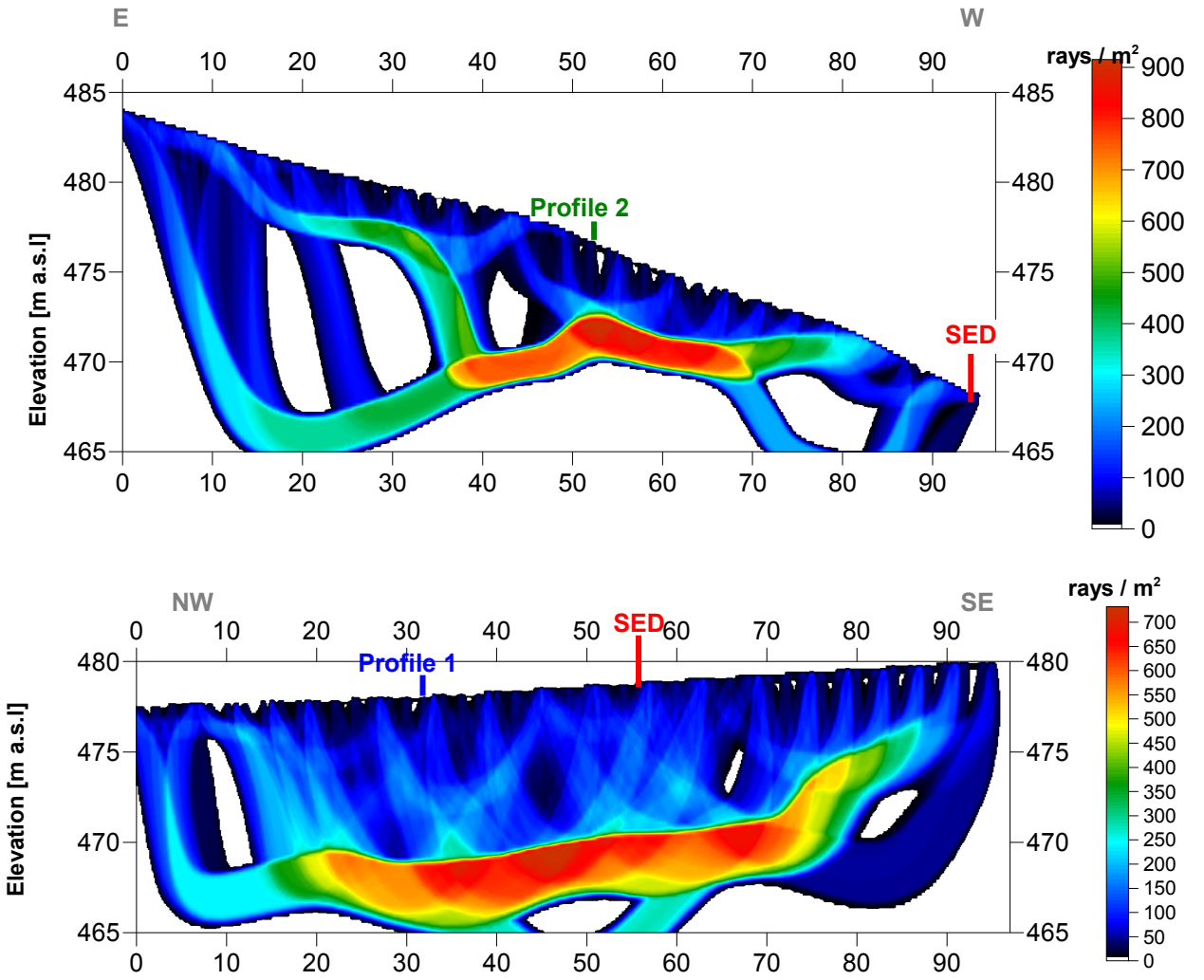

Fig. 3.2f: Shear wave ray path density along the seismic line 09SN_01ACB-S1 (top) and -S2 (bottom). Red/white colors indicate high velocity contrasts (usually at the bedrock surface), blue/black colors denote low coverage areas. Vertical axis: elevation [m a.s.l]; horizontal axis: profile meter; color encoded scale: ray paths per m²; vertical exaggeration: 2:1. The station spacing is 2 m, profile meter 0 = profile station 00, profile meter 96 = profile station 48.

Depth [m]	Vs [m/s]
0.0	274
0.5	257
1.1	295
1.6	370
2.2	467
2.7	582
3.2	702
3.8	793
4.3	827
4.9	693
5.4	588
5.9	559
6.5	589
7.0	728
7.6	880

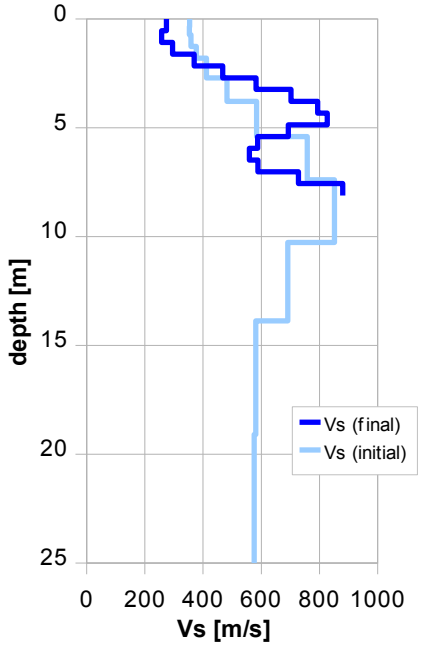

Tab. 3.2b: Final 1D s-wave velocity model derived from real data from line 09SN_01ACB-S1 (horizontal average of all values) for the profile segment (between profile meters 5 and 45) with a geological setting resembling the one at the SED station. The calculated values of the initial 1D s-wave velocity model are given in Tab. 3.2a.

Depth [m]	Vs [m/s]
0.0	266
0.7	293
1.4	339
2.1	389
2.8	418
3.5	440
4.2	489
4.9	559
5.6	611
6.3	630
7.0	649
7.7	693
8.4	763
9.1	862
9.8	934
10.5	1078

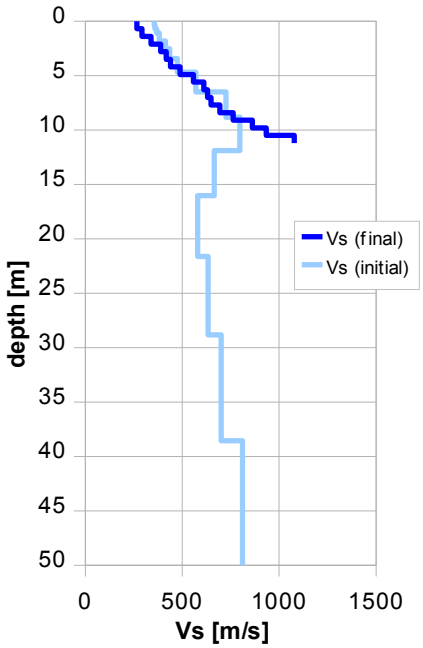

Tab. 3.2c: Final 1D s-wave velocity model derived from real data from line 09SN_01ACB-S2 (horizontal average of all values) for the profile segment (between profile meters 30 and 50) with a geological setting resembling the one at the SED station. The calculated values of the initial 1D s-wave velocity model are given in Tab. 3.2a.

The attained depth of investigation being limited to 11 m on line 09SN_01ACB-S2 is to be attributed to the method inherent constraining factor of critically refracted waves along the shallow bedrock surface (hard-kick), combined with the insufficient length of the lay-out spread for recording long offset data needed for deeper penetration.

3.3 MASW Processing

3.3.1 Reformatting and field geometry assignment

The data preparation steps for the dispersion analysis include

- the assignment of the field acquisition geometry
- the selection of suitable offset ranges (=arrays) between 10 m and 50 m for dispersion, and the splitting of the field records in forward and reverse shooting direction data sets
- the reformatting of the data into the specific KGS format

X - - ... - - o-o-o-...-o-o-o (forward shooting or so-called PLUS direction)
respectively
o-o-o-...-o-o-o - - ... - - X (reverse shooting or so-called MINUS direction).

where **X** = shot position
o = receiver station
- = 1.0 m offset

The active array used at SED-station ACB are the receiver station in the shot offset range between 10 and 50 m.

3.3.2 Calculating the dispersion image (overtone)

The result of dispersion analysis is the color encoded acoustic energy distribution in the phase velocity - frequency plane (see Fig. 3.3a and b).

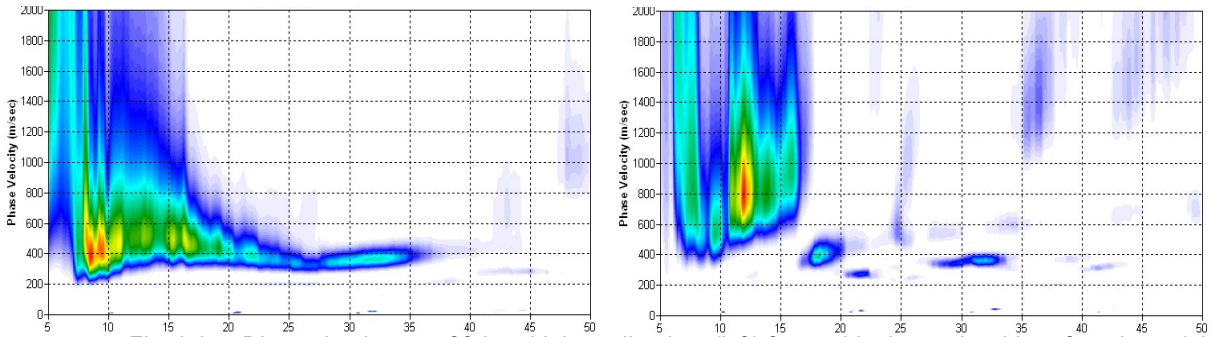

Fig. 3.3a: Dispersion image of fair to high quality data (left) from midpoint station 22 as found on 40 % and of deficient quality data (right) from midpoint station 53 representing about 60 % of the MASW dataset of site ACB.
Horizontal axis: frequency from 5 to 50 Hz; vertical axis: phase velocity from 0 to 2000 m/s; color code: colors from white (no energy) to blue - green - yellow - red - black point to increasing energy amplitude values.

3.3.3 Analysis of the dispersion image

In the dispersion graphs as calculated in section 3.3.2 above, the curves joining the amplitude peaks of the fundamental modes are determined either by subjective inspection or in a semi-automated manner. On datasets with poorly defined amplitude peaks or with a highly irregular alignment of the peaks, the danger of obtaining improbable or wrong results is real and can only be mitigated by the processing experience and the a-priori knowledge of the geological setting by the geophysicist responsible for the data evaluation.

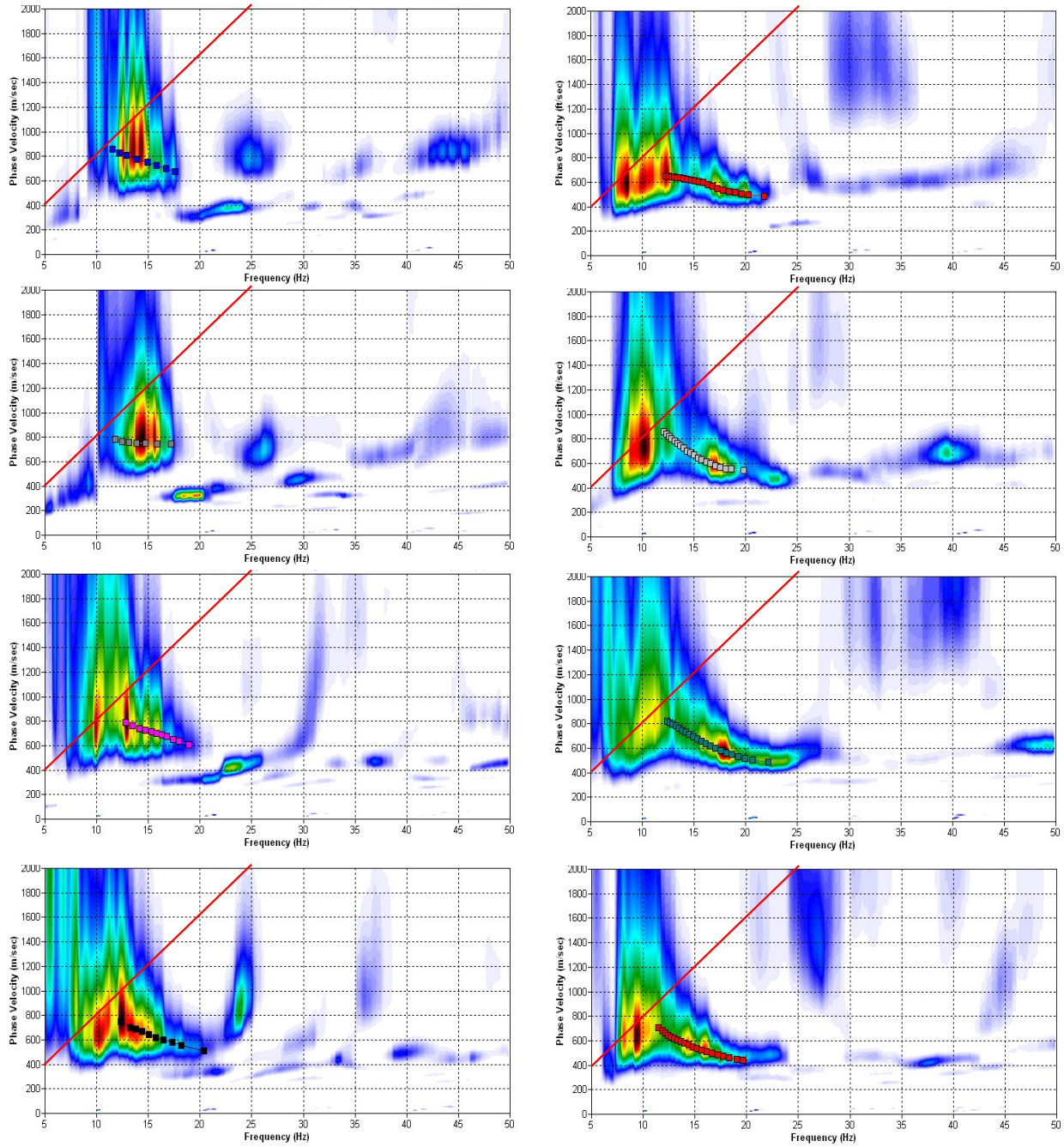

Fig. 3.3b: The manually picked dispersion images used for the derivation of the shear wave velocity section on line 09SN_01ACB-M1. The dispersion curves (squares) are determined by linking the peaks of high energy. Note that 'higher modes' may at times produce higher energy peaks than the fundamental mode required for the analysis.
dotted fine line: signal-noise ratio for the designated f-v_{ph} – value.
red line: high resolution beam-forming curve for v_{max}.
1st row: left: station 44 @ PLUS direction; right: station 46 @ MINUS direction
2nd row: left: station 50 @ PLUS direction; right: station 54 @ MINUS direction
3rd row: left: station 62 @ PLUS direction; right: station 60 @ MINUS direction
4th row: left: station 65 @ PLUS direction; right: station 66 @ MINUS direction

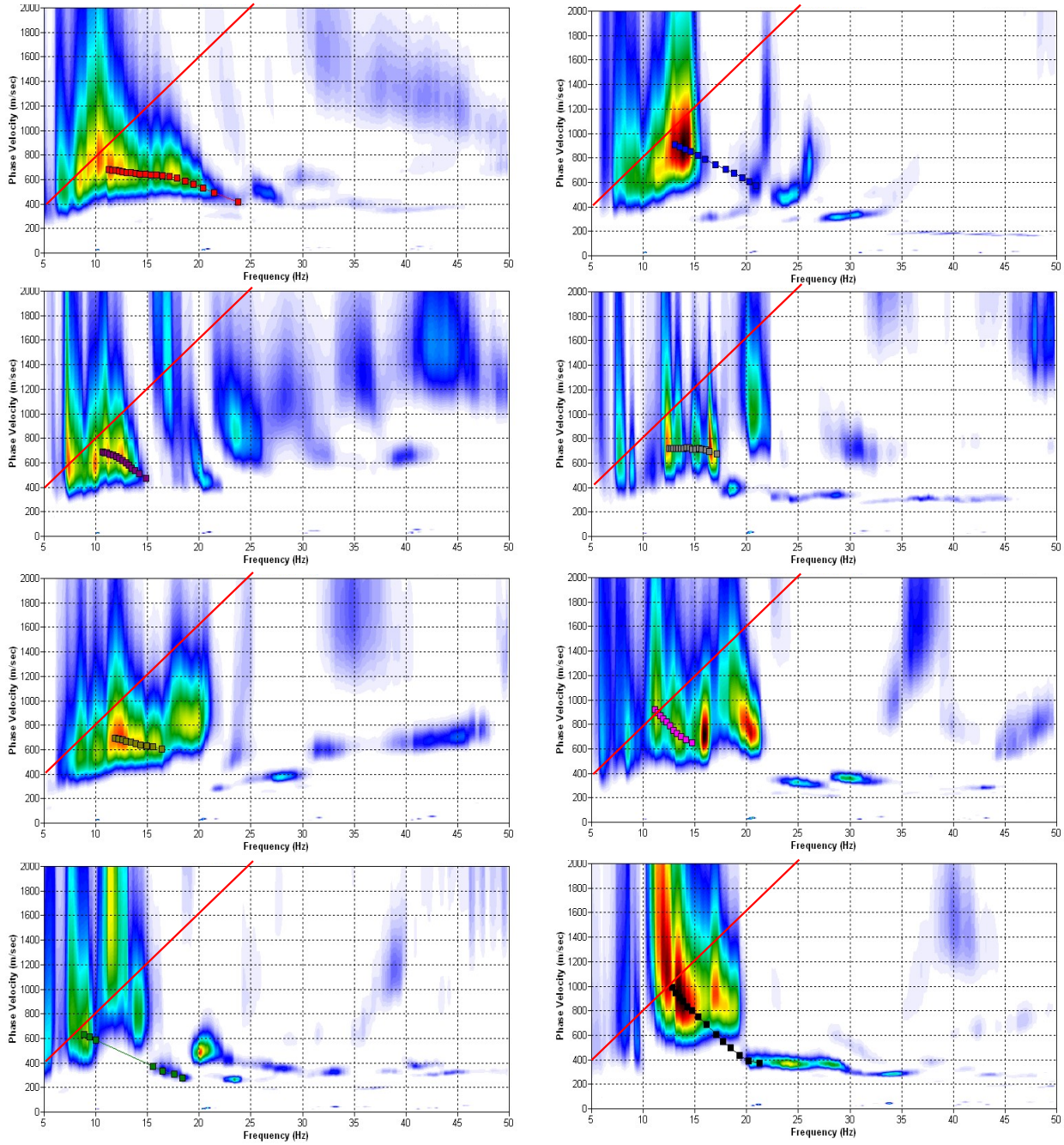

Fig. 3.3c: The manually picked dispersion images used for the derivation of the shear wave velocity section on line 09SN_091ACB-M2. The dispersion curves (squares) are determined by linking the peaks of high energy. Note that 'higher modes' may at times produce higher energy peaks than the fundamental mode required for the analysis.
dotted fine line: signal-noise ratio for the designated f-v_{ph} – value.
red line: high resolution beam-forming curve for v_{max}.
1st row: left: station 28 @ PLUS direction; right: station 31 @ MINUS direction
2nd row: left: station 40 @ PLUS direction; right: station 41 @ MINUS direction
3rd row: left: station 49 @ PLUS direction; right: station 47 @ MINUS direction
4th row: left: station 58 @ PLUS direction; right: station 56 @ MINUS direction

3.3.4 Inversion of dispersion curves resulting in a 1D shear wave velocity distribution

Inversion of the extracted dispersion curves was performed using the algorithm described by Xia et al. (1999).

The inversion process is started by setting the maximum depth (z_{max}) to be in the order of 30% of the largest wavelength for an initial model consisting of 10 layers of increasing thicknesses. For all 10 layers the Poisson's ratio is assumed to be 0.4 and the rock/soil density to be 2.0 g/cm^3. The inversion process is concluded either after twelve iterations or when the convergence condition of a RMS-error of less than 3 m/s (phase velocity) is met.

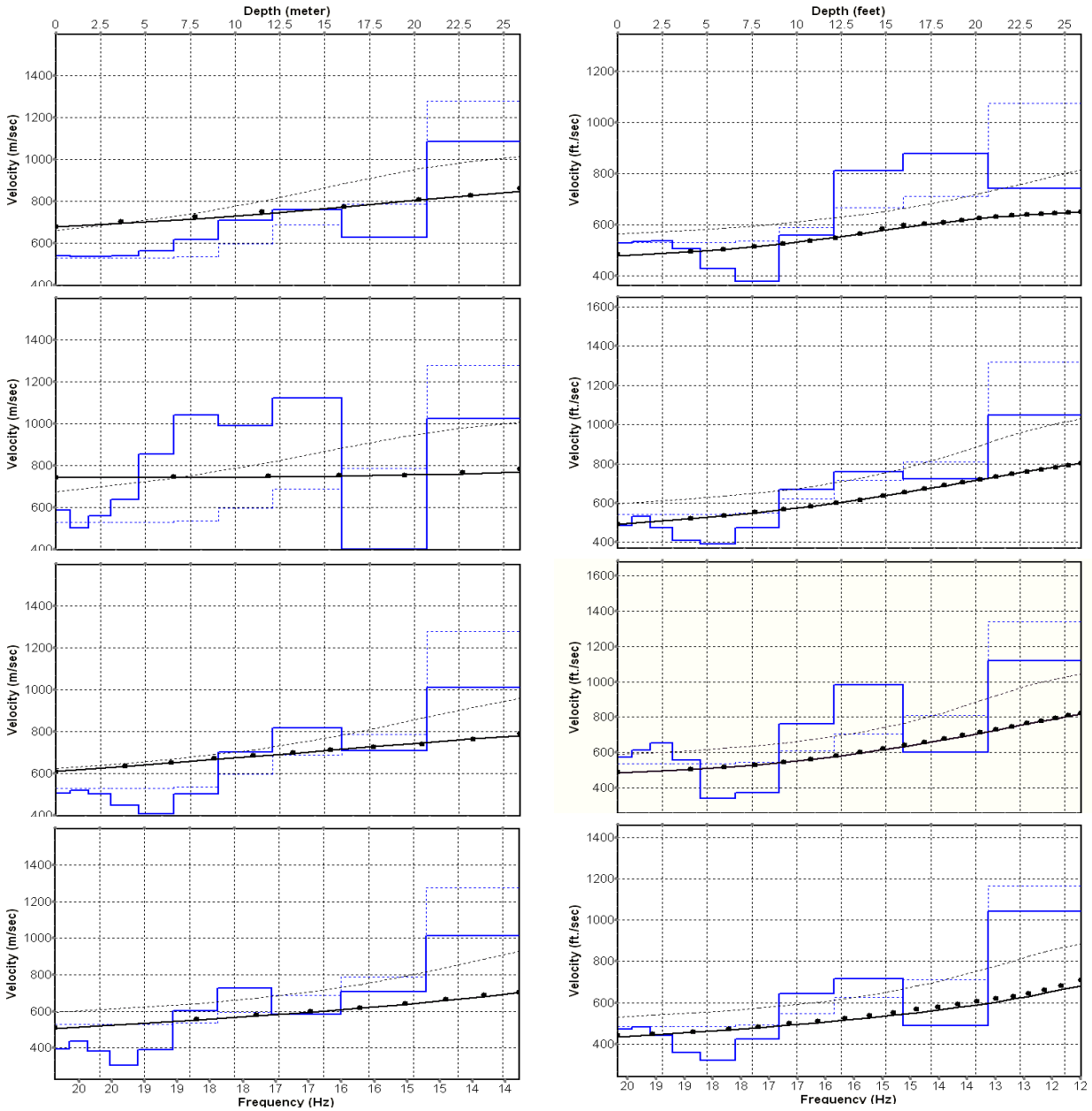

Fig. 3.3d: Inversion results of dispersion curves from dataset at line 09SN_01ACB-M1.
***brown**: Inversion of dispersion curve (dots) resp. of the modeled dispersion curve (dotted line: initial model; continuous line: end model). Horizontal axis: frequency Hz, vertical axis: v_s.*
***blue**: 10-layer-model (dotted: initial model, continuous line: final model). Horizontal axis: depth, vertical axis: phase velocity resp. v_S).*
1st row: left: station 44 @ PLUS direction; right: station 46 @ MINUS direction
2nd row: left: station 50 @ PLUS direction; right: station 54 @ MINUS direction
3rd row: left: station 62 @ PLUS direction; right: station 60 @ MINUS direction
4th row: left: station 65 @ PLUS direction; right: station 66 @ MINUS direction

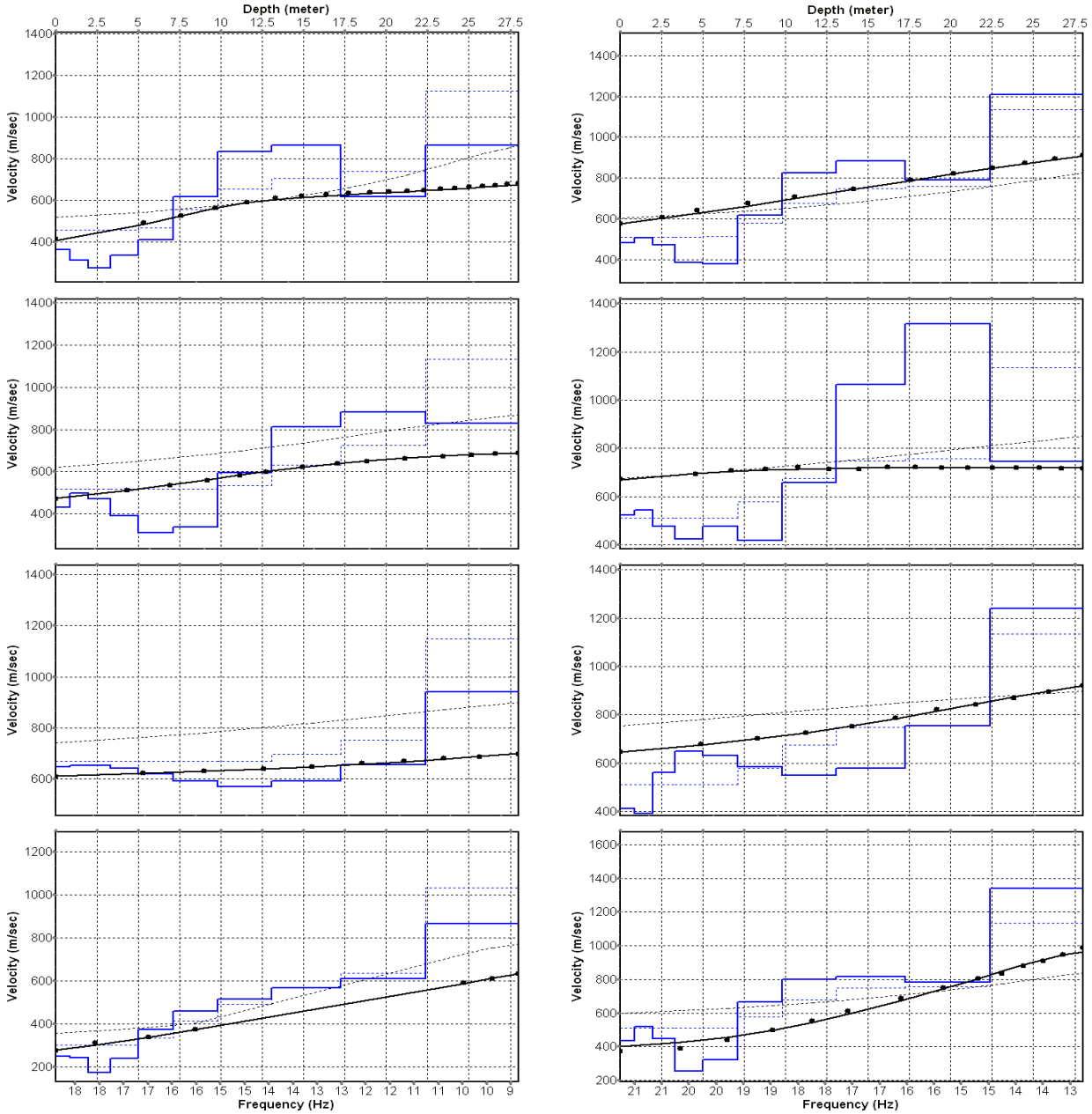

Fig. 3.3e: Inversion results of dispersion curves from dataset at line 09SN_01ACB-M2.
***brown**: Inversion of dispersion curve (dots) resp. of the modeled dispersion curve (dotted line: initial model; continuous line: end model). Horizontal axis: frequency Hz, vertical axis: v_s.*
***blue**: 10-layer-model (dotted: initial model, continuous line: final model). Horizontal axis: depth, vertical axis: phase velocity resp. v_S).*
1st row: left: station 28 @ PLUS direction; right: station 31 @ MINUS direction
2nd row: left: station 40 @ PLUS direction; right: station 41 @ MINUS direction
3rd row: left: station 49 @ PLUS direction; right: station 47 @ MINUS direction
4th row: left: station 58 @ PLUS direction; right: station 56 @ MINUS direction

Dispersion analyses of records with longer receiver arrays should – by theory – increase the investigation depth. At ACB, with both lines and both directions, MASW processing with the maximal array length of 96 m doesn't improve the results (Fig. 3.3f and 3.3g).

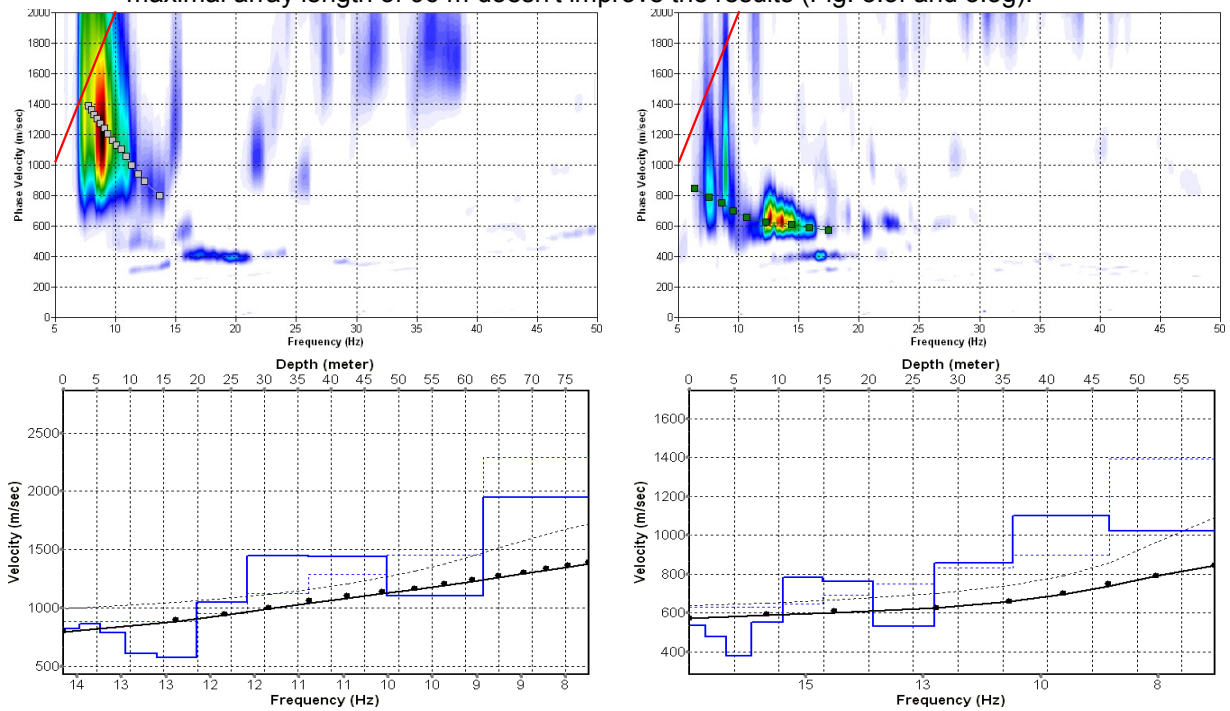

Fig. 3.3f: Top: dispersion images of over-all arrays (10...106 m offset) from line 09SN_01ACB-M1 in PLUS (left) and MINUS (right) direction; dotted fine line: signal-noise ratio for the designated f-v_{ph}-value. Red line: high resolution beam-forming curve for v_{max}.
*Below: The two respective inversion results; **brown**: inversion of dispersion curve; **blue**: 10-layer-model. Horizontal axis: depth, vertical axis: phase velocity resp. v_s.*

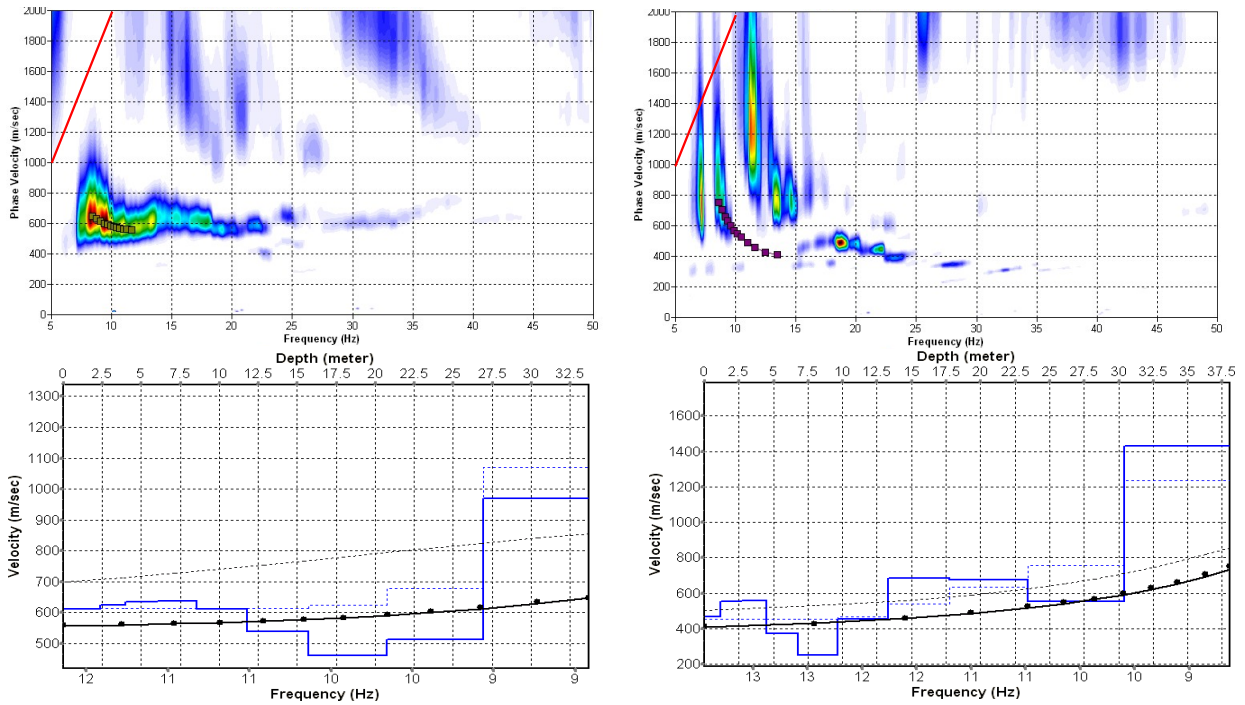

Fig. 3.3g: Top: dispersion images of over-all arrays (10...106 m offset) from line 09SN_01ACB-M2 in PLUS (left) and MINUS (right) direction; dotted fine line: signal-noise ratio for the designated f-v_{ph} – value. Red line: high resolution beam-forming curve for v_{max}.
*Below: The two respective inversion results; **brown**: inversion of dispersion curve; **blue**: 10-layer-model. Horizontal axis: depth, vertical axis: phase velocity resp. v_s.*

3.3.5 Gridding and plotting of 2D v_s-velocity field

By assembling the 1D v_s - depth functions from all stations the final 2D v_s-field is derived using a Kriging gridding procedure as portrayed in Fig. 3.3h and 3.3i below:

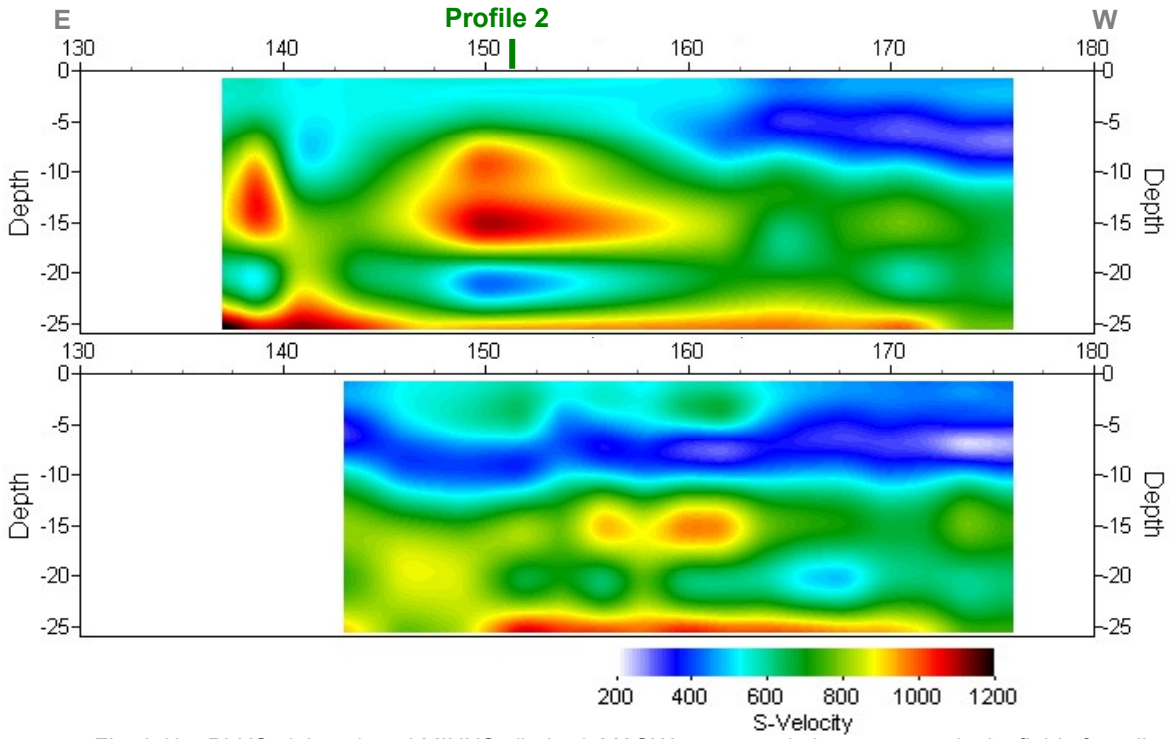

Fig. 3.3h: PLUS- (above) and MINUS- (below)-MASW-processed shear wave velocity fields from line 09SN_01ACB-M1. Profile station number 150 = profile meter 50, station spacing is 1 m.

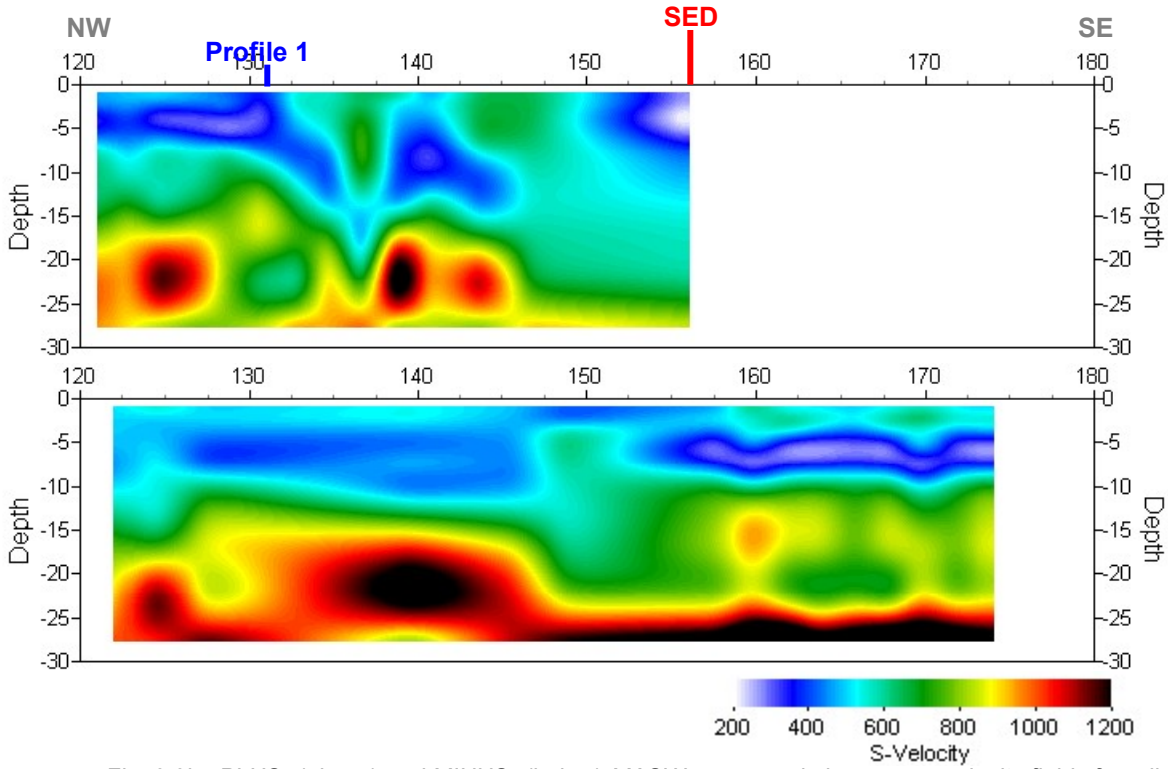

Fig. 3.3i: PLUS- (above) and MINUS- (below)-MASW-processed shear wave velocity fields from line 09SN_01ACB-M2. Profile station number 150 = profile meter 50, station spacing is 1 m.

3.3.6 Calculation of the average shear wave velocity

In order to calculate a representative shear wave velocity-depth function from line 09SN_01ACB-M1 at the SED station, all computed 1D-v_S-depth functions between seismic profile station no. 45 and 65 – that are four profiles in each direction – are averaged (non-weighted mean values). The v_S-depth-function is shown in Tab. 3.3a.

Depth [m]	Vs+ [m/s]	Vs- [m/s]	Vs [m/s]
0.9	469	515	492
2.0	488	515	501
3.3	484	491	488
5.0	433	478	455
7.1	449	487	468
9.8	547	505	526
13.1	687	568	627
17.2	843	713	778
22.4	940	825	882
28.0	1131	876	1003

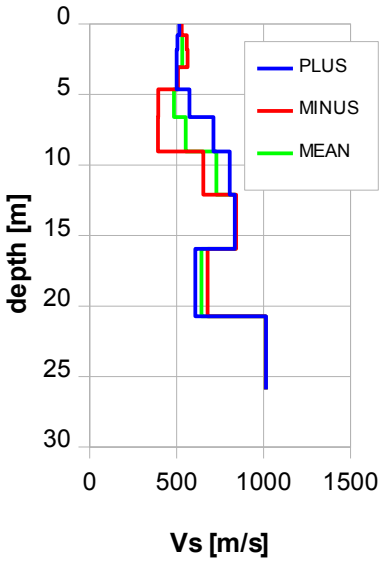

Tab. 3.3a: Averaged vs - depth function from line 09SN_01ACB-M1 at the SED station ACB. Blue line: MASW-'PLUS' processing, red line: MASW-'MINUS' processing; green line: average of PLUS- and MINUS-functions.

In order to calculate an representative shear wave velocity-depth function from line 09SN_01ACB-M2 at the SED station, all computed 1D-v_S-depth functions between seismic profile station no. 30 and 55 are averaged (non-weighted mean values). The resulting v_S-depth-function is shown in Tab. 3.3b.

Depth [m]	Vs- [m/s]	Vs+ [m/s]	Vs [m/s]
0.8	529	515	522
1.8	558	505	532
3.1	563	500	532
4.6	507	500	504
6.6	394	573	484
9.0	393	711	552
12.1	653	805	729
15.9	842	834	838
20.7	678	608	643
25.9	1012	1014	1013

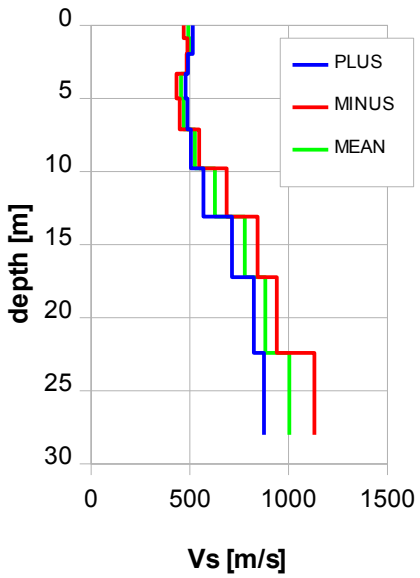

Tab. 3.3b: Averaged v_S - depth function from line 09SN_01ACB-M2 at the SED station ACB. Blue line: MASW-'PLUS' processing, red line: MASW-'MINUS' processing; green line: average of PLUS- and MINUS-functions.

The inversion of the four 100 m-array dispersion curves data (10 to 106 m offset, see Fig. 3.3f and 3.3g) are given in Tab. 3.3c. These values are complemented with the values derived from the 40 m-arrays analyses (Tab. 3.3a and 3.3b).

100 m array								40 m array				
depth	m1+	m1-	m2+	m2-	m1	m2	m	depth	m1	depth	m2	depth
1.6	820	535	611	469	678	540	655	0.8	515	0.9	529	0.8
3.6	860	475	612	552	668	582	649	1.8	505	2.0	558	1.8
6.2	788	378	625	557	583	591	597	3.1	500	3.3	563	3.1
9.3	605	552	636	371	579	503	598	4.6	500	5.0	507	4.6
13.3	571	781	637	249	676	443	663	6.6	573	7.1	394	6.6
18.2	1050	761	612	453	905	533	808	9.0	711	9.8	393	9.0
24.4	1442	532	538	686	987	612	837	12.1	805	13.1	653	12.1
32.1	1440	856	460	677	1148	569	919	15.9	834	17.2	842	15.9
41.8	1102	1102	512	555	1102	533	905	20.7	608	22.4	678	20.7
52.2	1947	1021	969	1430	1484	1199	1312	25.9	1014	28.0	1012	25.9

Tab. 3.3c: v_s-depth values from the four MASW-derived dispersion curves of both seismic line 09SN_01ACB-M1 and 09SN_01ACB-M2 using 100 m-arrays. The dispersion curves are shown in Fig. 3.3f and Fig 3.3g.

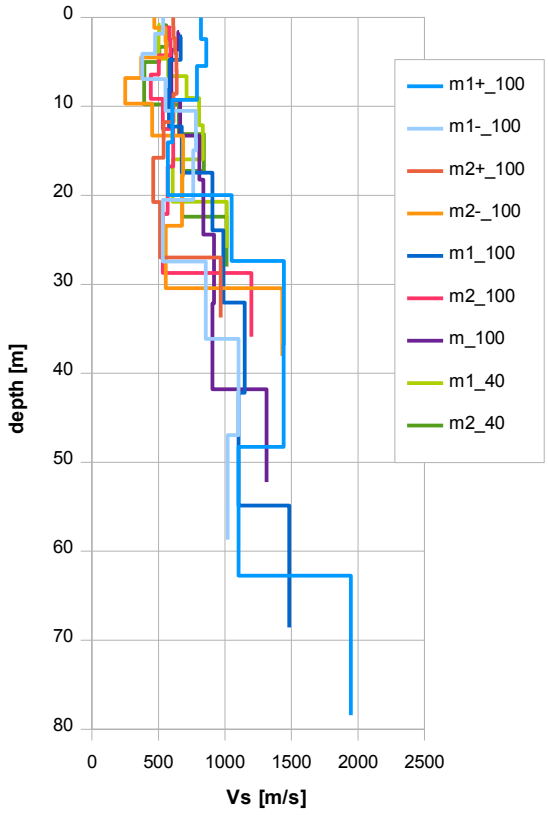

Fig. 3.3j: Comparison of the ensemble of inversion results of both lines 09SN_01ACB-M1 and -M2, either using the 40 m- and the 100 m-arrays.
blue lines: analyses of records from line 09SN_01ACB-M1
red lines: analyses of records from line 09SN_01ACB-M2
violet line: mean of both 100 m-array records analyses in MINUS and PLUS direction.
green lines: v_s-values from analyses of 40 m-array records.

3.3.7 Calculation of the shear wave velocity scalars $v_{s,5}$, $v_{s,10}$, ...

The parameters $v_{s,5}$, $v_{s,10}$, $v_{s,20}$, $v_{s,30}$, $v_{s,40}$, $v_{s,50}$ represent the average shear wave velocities in the depth interval between the surface and the respective depth levels and are determined from the formula

$$v_{s,n} = \frac{\sum_{i=1}^{n} d_i}{\sum_{i=1}^{n} d_i / v_{si}}$$

with:

d_i = thickness of layer i

v_{si} = corresponding shear-wave velocity.

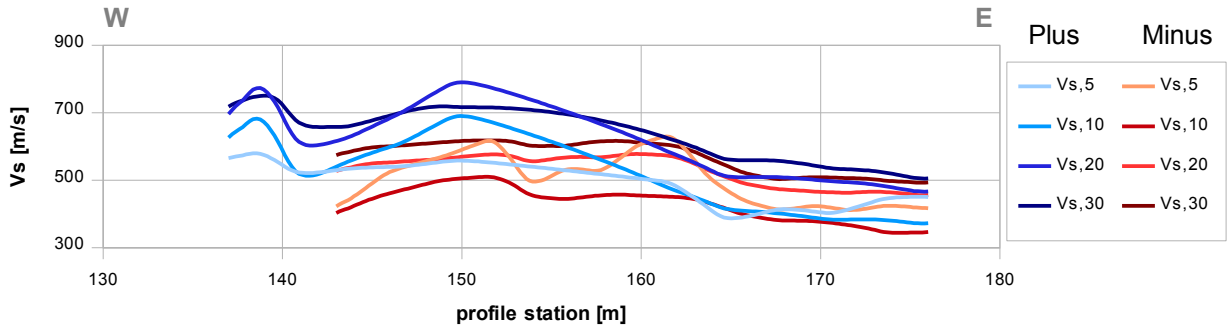

Fig. 3.3k: Graphs of the averaged vs,5...-values along the line 09SN_01ACB-M1 for the PLUS- (blue lines) and MINUS- (red lines) directions.

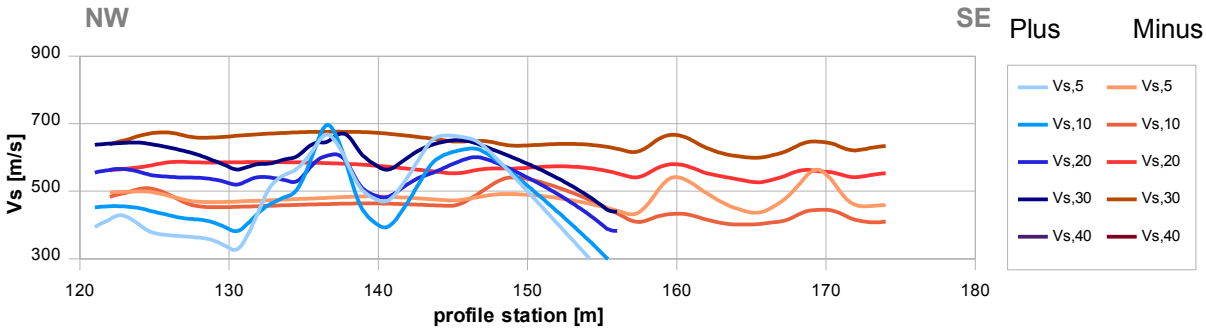

Fig. 3.3l: Graphs of the averaged $v_{s,5}$...-values along the line 09SN_01ACB-M2 for the PLUS- (blue lines) and MINUS- (red lines) directions.

The average values of the s-wave velocity model $v_{s,5}$, $v_{s,10}$, $v_{s,20}$, $v_{s,30}$, $v_{s,40}$, $v_{s,50}$, $v_{s,100}$ (= average shear wave velocity from the surface to depths of 5 m, …until 100 m) on the line segment nearest to the SED station (Tab. 3.3d) are summarized below:

	Vs,5	Vs,10	Vs,20	Vs,30	Vs,40	Vs,50
MINUS	550	462	559	599	n/a	n/a
PLUS	511	571	671	669	n/a	n/a
MEAN	530	516	615	634	n/a	n/a

	Vs,5	Vs,10	Vs,20	Vs,30	Vs,40	Vs,50
MINUS	477	476	572	656		n/a
PLUS	496	480	539	606		n/a
MEAN	487	478	556	631		n/a

Tab. 3.3d: The average shear wave velocities within the depth intervals from surface down to 5 m, etc.… to 50 m, calculated for the line segment with a subjectively most similar geology to the SED station (profile station 45 to 65 for line 09SN_01ACB-M1, above; profile stations 30 to 55 for line 09SN_01ACB-M2, below).

3.4 Hybrid Seismic Data Processing

3.4.1 p-wave *Reflection* Seismic Processing Sequence

A) Data conditioning

A1 Reformatting and quality verification of field data
A2 Recording geometry assignment
A3 Data editing (suppression of bad / dead traces, etc.)
A4 Preliminary analysis of refraction velocities

B Filtering and deconvolution

B1 Analytical muting of refraction arrivals
B2 Amplitude recovery / amplitude equalization in time and frequency domains
B3 Predictive deconvolution parameter tests / application
B4 Determination of band limiting corner frequencies / application
B5 Optional 2-D filtering

C) Velocity analysis and stack

C1 Common Depth Point (CDP) sort
C2 Semblance velocity analysis using supergathers of 3 - 5 CDP's
C3 Optional dip move-out correction
C4 Normal Move-Out (NMO) correction and application of stretch mute
C5 Band-pass filtering
C6 CDP stack
C7 Optional coherency filtering

D) Time-depth conversion

D1 Optional spiking deconvolution
D2 Band-pass filtering
D3 Depth conversion
D4 Final display of seismic depth section with inversed polarity (non-SEG-convention)

3.4.2 The presentation of reflection seismic data

The data in a reflection seismic section are presented as an assembly of individual seismic signals at regular intervals along a seismic profile. The simplest way of representing the signals are single wiggle lines (first to the left in the illustration below). A more capturing presentation is the variable area form (second to the left). Combining these two modes results in the var-wiggle mode. Another method of data visualization is the variable density mode (second from the right).

The compressional phase of seismic signals is defined in this report as the onset of the positive amplitude excursion in black (Fig. 3.4a). Since the source signal is produced by an explosion or by an impact at the surface, the signal starts off with a compression of the ground particles. Thus the arrivals of reflection events are defined by the compressional phase.

In rare situations of velocity inversions, cases in which formation velocities are lower than in the layers above, polarity reversals of the reflected signals occur. The beginning of the reflection event would then be characterized by a dilatational phase, represented in this report as a negative amplitude excursion, i.e. in white.

The final p-wave seismic depth sections are displayed in Fig. 3.4b and 3.4c, the hybrid sections in Fig. 3.4j and -k further below.

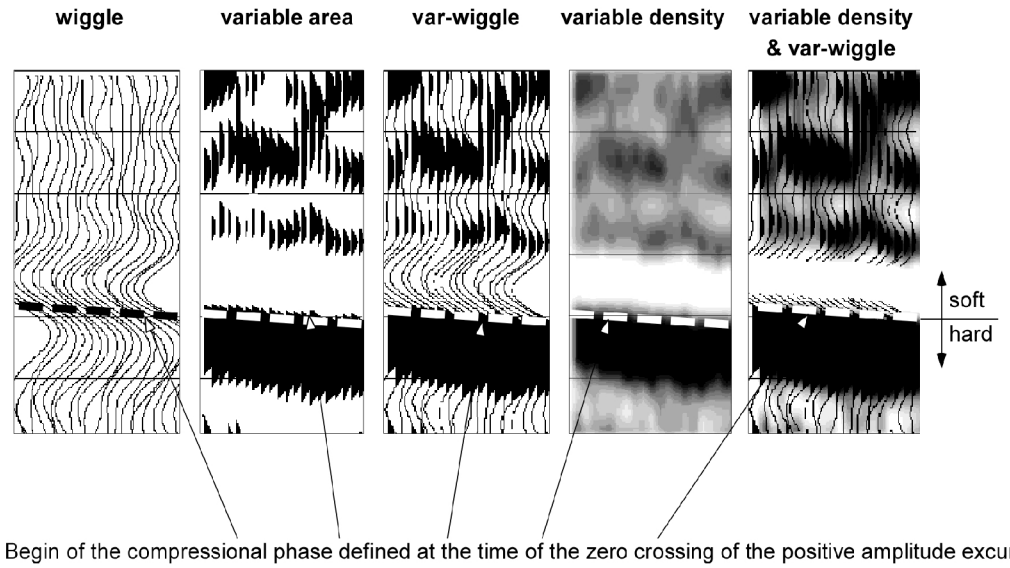

Fig. 3.4a Representation of reflection seismic data and the definition of a reflection event.

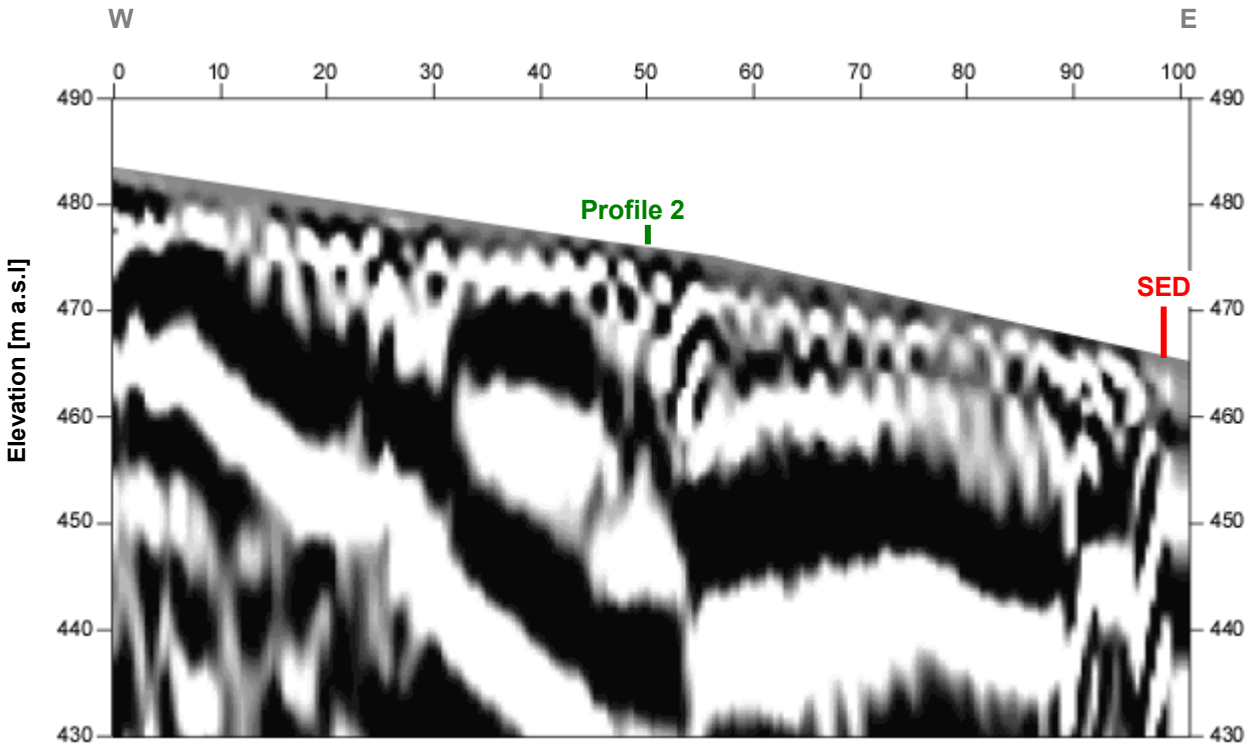

Fig. 3.4b: Seismic depth section of seismic line 09SN_01ACB-P1 with variable density mode presentation. Vertical axis: elevation [m a.s.l.], horizontal axis: profile meter; no vertical exaggeration. The station spacing is 1 m.

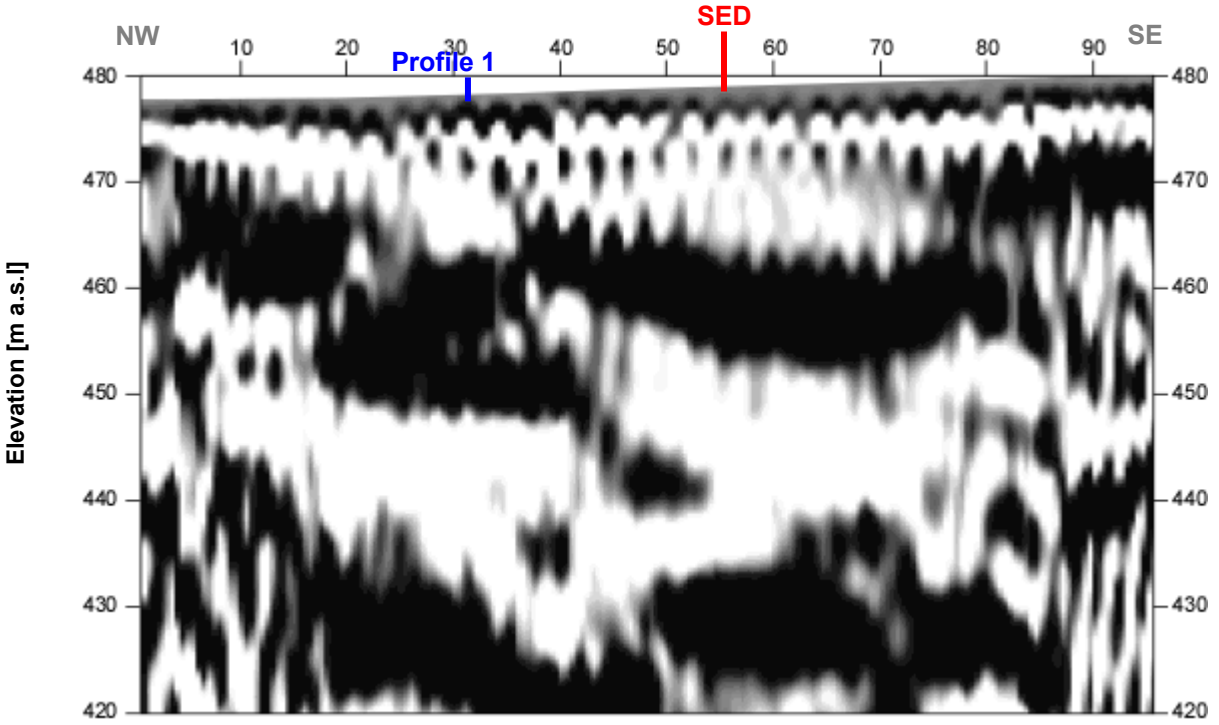

Fig. 3.4c: Seismic depth section of seismic line 09SN_101ACB-P1 with variable density mode presentation. Vertical axis: elevation [m a.s.l.], horizontal axis: profile meter; no vertical exaggeration. The station spacing is 1 m.

3.4.3 p-wave refraction tomography processing

The seismic p-wave refraction processing steps are analogous to those described in paragraph 3.2. For a detailed method statement and a description of the processing steps please refer to the summary report. The Figs. 3.4d to 3.4i and Tab. 3.4a illustrate the intermediate processing steps and the final result.

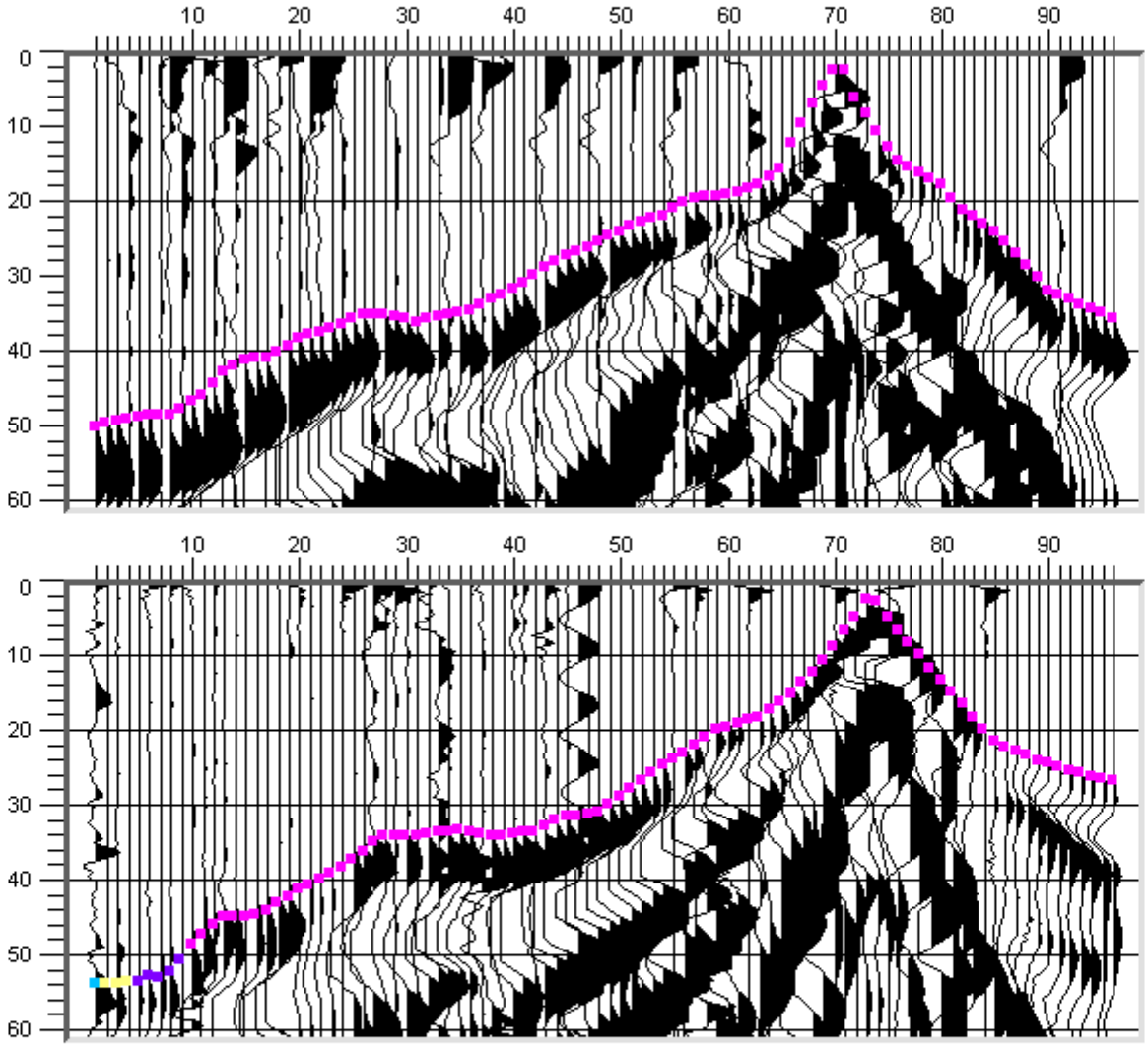

Fig. 3.4d: p-wave records from 09SN_01ACB-P1 (above) and -P2 (below) with positive amplitude excursions in black. Colored dots mark the manually picked first break arrival times. Vertical axis: travel time in ms, horizontal axis: station numbers spaced at 1 m.

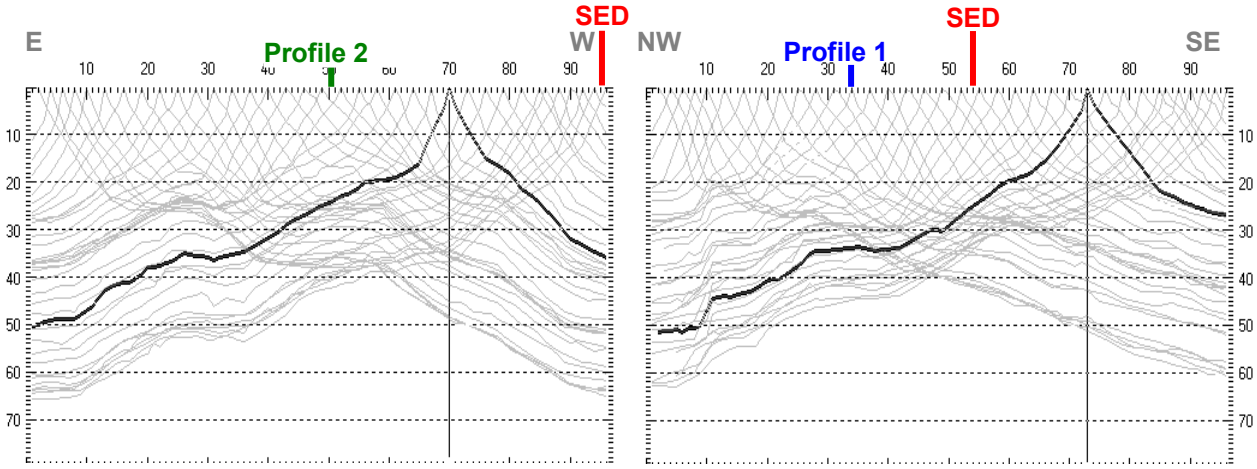

Fig. 3.4e: Travel time curves of p-wave arrival time picks from line 09SN_01ACB-P1 (left) and -P2 (right). Vertical axes: travel time [ms], horizontal axes: station number (= profile meter).

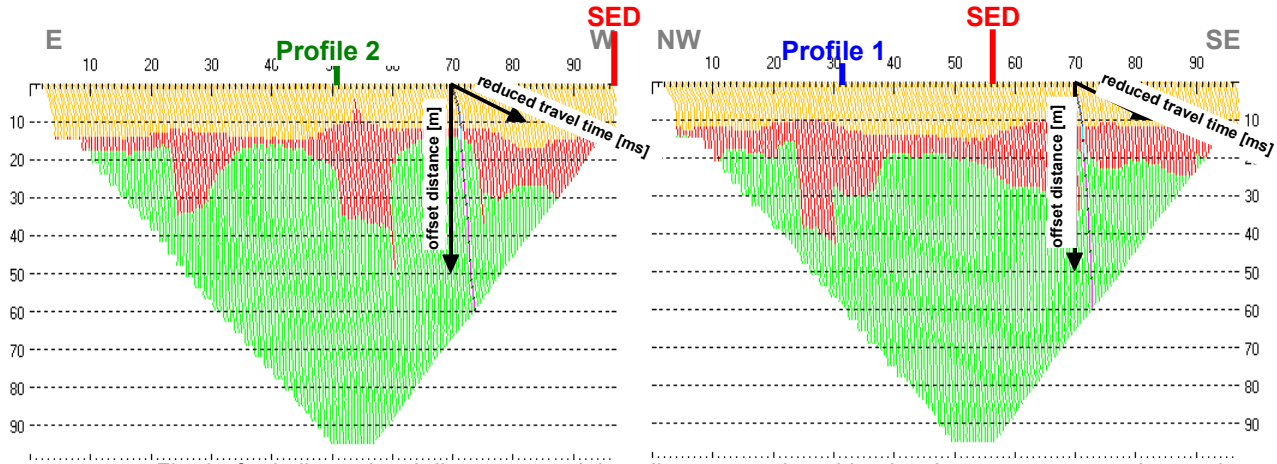

Fig. 3.4f: 3-dimensional distance-travel time diagrams at the mid-points between source points and receiver stations are instrumental when using the analytical CMP derivation of the initial velocity field. The horizontal axes are along the CMP positions and the travel time respectively, the vertical axis denotes the offset distance between source and receiver positions.

Depth [m]	Vp [m/s]
0.2	422
0.5	514
0.9	548
1.4	597
2.0	669
2.9	829
3.9	1215
5.3	1846
7.2	2228
9.6	1616
12.6	1471
16.5	1808
21.7	2374
28.3	2752
37.0	3817
48.3	4656

Depth [m]	Vp [m/s]
	390
0.2	441
0.5	499
0.8	516
1.4	543
2.0	613
2.9	726
3.9	880
5.2	1125
7.1	1483
9.5	2153
12.5	3216
16.4	3221
21.5	2880
28.1	2683
36.7	3058

Tab. 3.4a: Initial 1D p-wave velocity model derived from real data (left: 09SN_01ACB-P1; right: -P2).

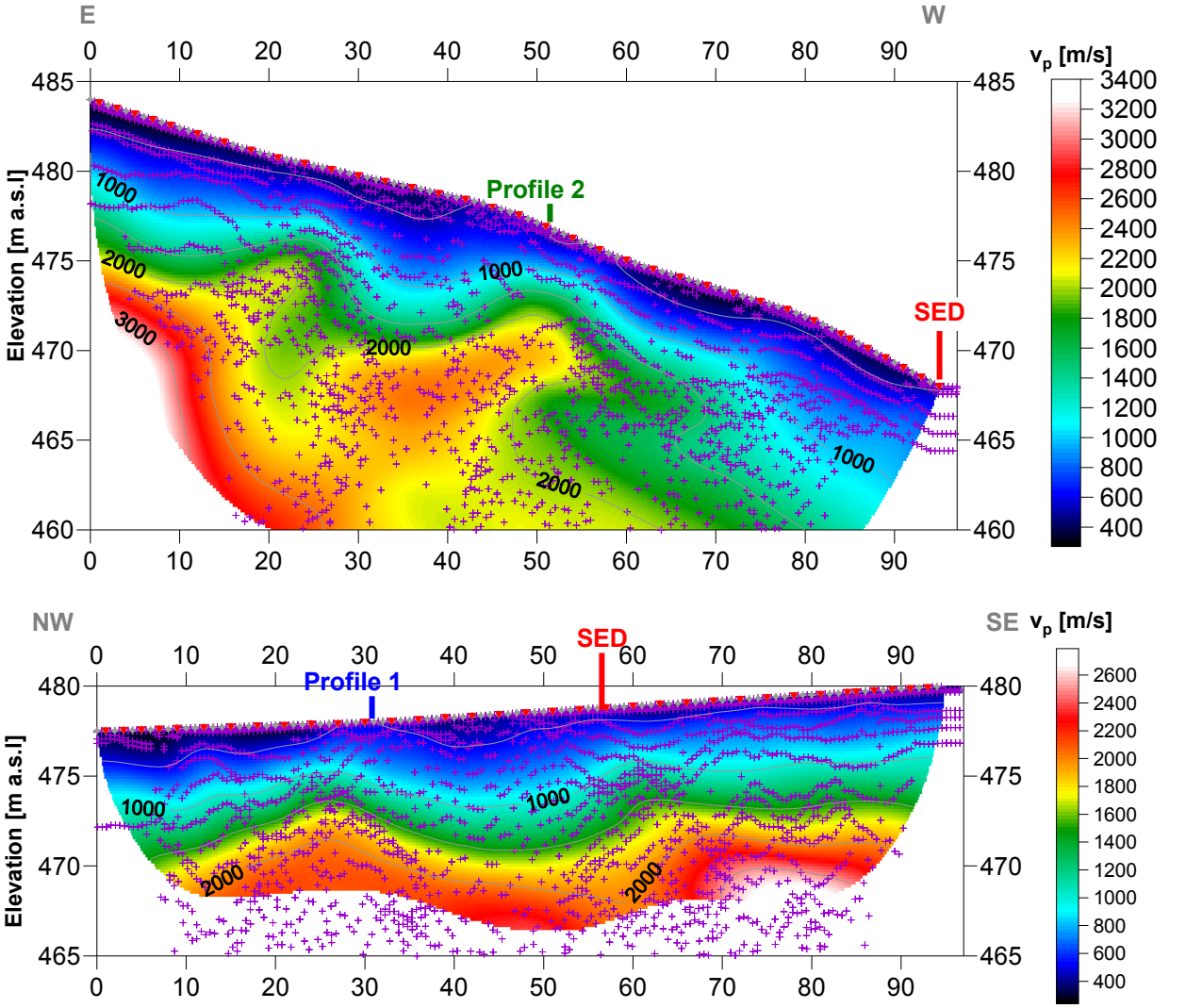

Fig. 3.4g: Compressional wave velocity field image along the seismic profiles 09SN-01ACB-P1 (above) and -P2 (below). Red/white colors indicate solid rock, blue/black colors unconsolidated sediments and soil. Vertical axis: elevation [m a.s.l]; horizontal axis: profile meter; color scale: v_s [m/s]; vertical exaggeration: 2:1; gray squares: receiver stations; red triangles: shot positions; magenta crosses: positions of determined velocity values.

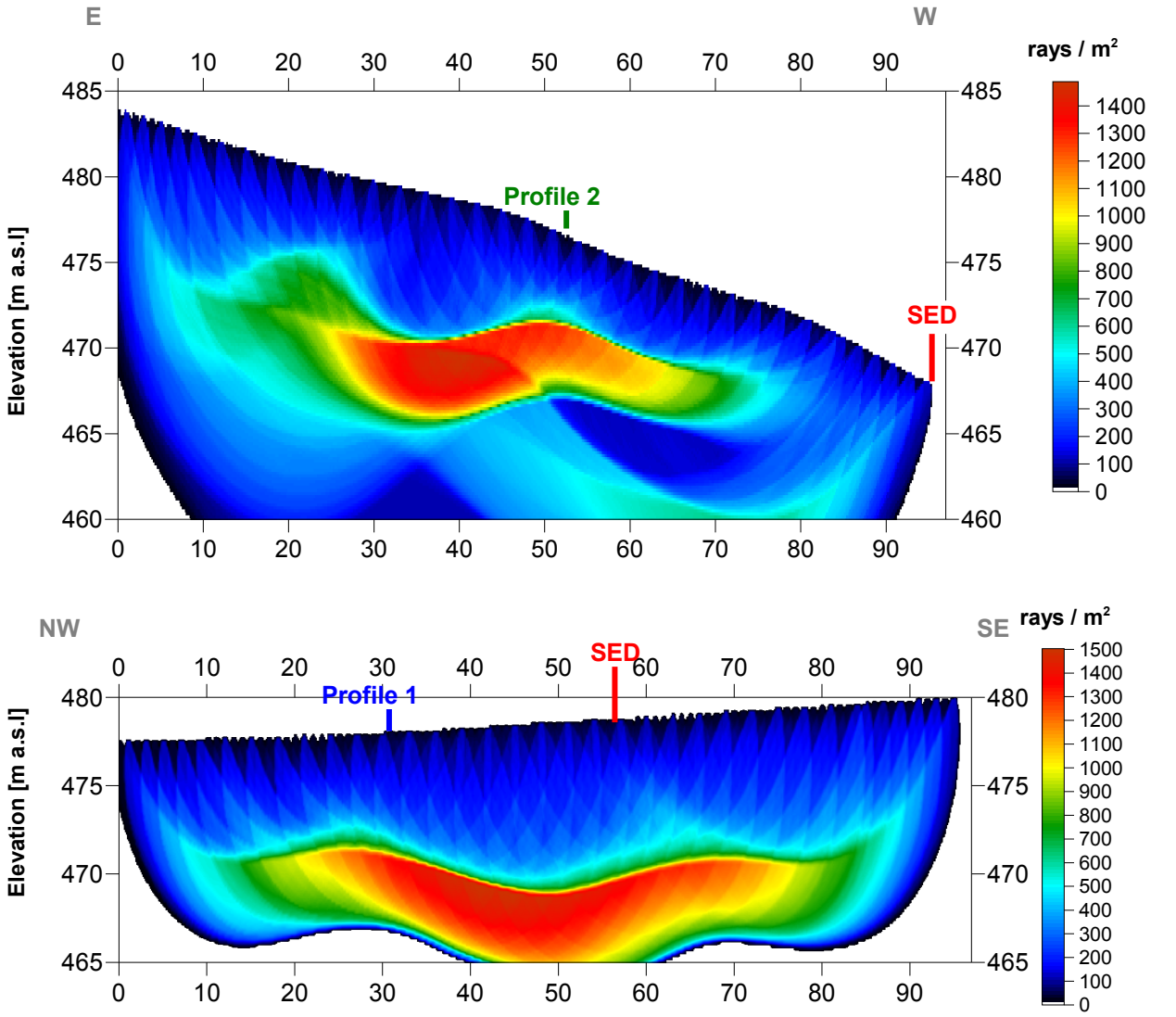

Fig. 3.4h Compressional wave subsurface ray path density along the seismic profiles 09SN_01ACB-P1 (above) and -P2 (below). Red/white colors indicate high velocity contrast between two layers, blue/black colors low coverage areas. Vertical axis: elevation [m a.s.l]; horizontal axis: profile meter; color scale: ray paths per m2; vertical exaggeration: 2:1.

Depth [m]	Vp [m/s]
0.0	495
1.2	620
2.2	847
3.2	1129
4.3	1441
5.3	1729
6.3	1939
7.3	2027
8.4	1949
9.4	1802
10.4	1763
11.4	1812
12.4	1895
13.5	1968
14.5	2020
15.5	2061
16.5	2086
17.6	2093
18.6	2083

Depth [m]	Vp [m/s]
0.0	420
0.7	465
1.4	533
2.0	604
2.7	694
3.4	805
4.1	940
4.7	1091
5.4	1247
6.1	1409
6.8	1575
7.4	1738
8.1	1880
8.8	1999
9.5	2079
10.2	2151
10.8	2234
11.5	2311

Tab. 3.4b: Final 1D p-wave velocity model derived from real data at positions most similar to the geological setting at SED station between profile meters 45 and 65 at line 09SN_01ACB-P1 (left) resp. 30 and 55 at line 09SN_01ACB-P2 (right) .

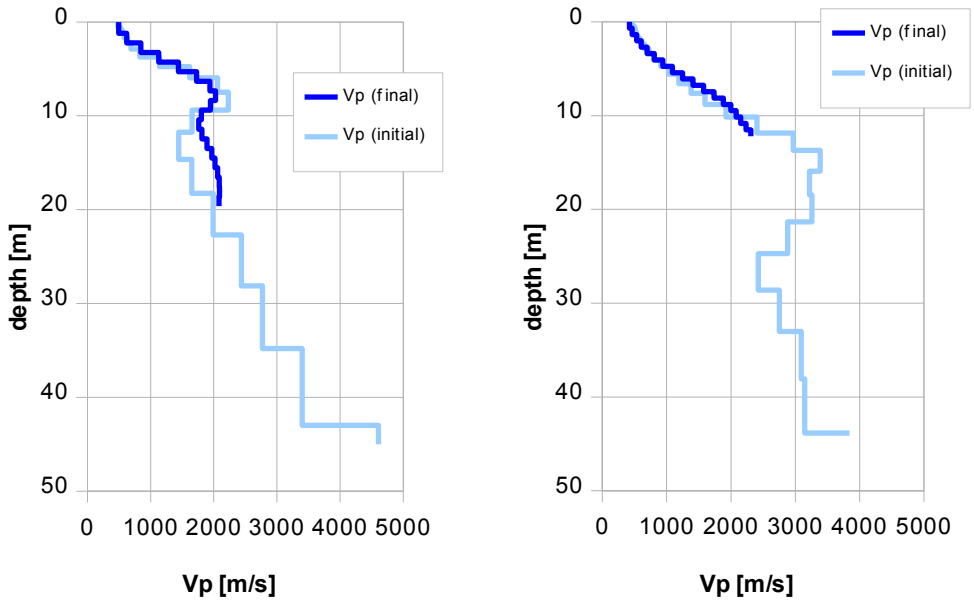

Fig. 3.4i: Final 1D p-wave velocity model derived from real data at a position most similar to the geological setting at the SED station between profile meters 45 and 65 at line 09SN_01ACB-P1 (left) resp. 30 and 55 at line 09SN_01ACB-P2 (right). Initial 1D p-wave velocity model values are given in Tab. 3.4a.

3.4.4 Representation of the hybrid seismic section

The hybrid seismic section is the reflection seismic section with the superimposed p-wave velocity field. It portrays the geological structures and the p-wave velocity field, the latter being indicative for the rock / soil rigidity. The uninterpreted hybrid seismic section is portrayed in Fig. 3.4j and 3.4k below.

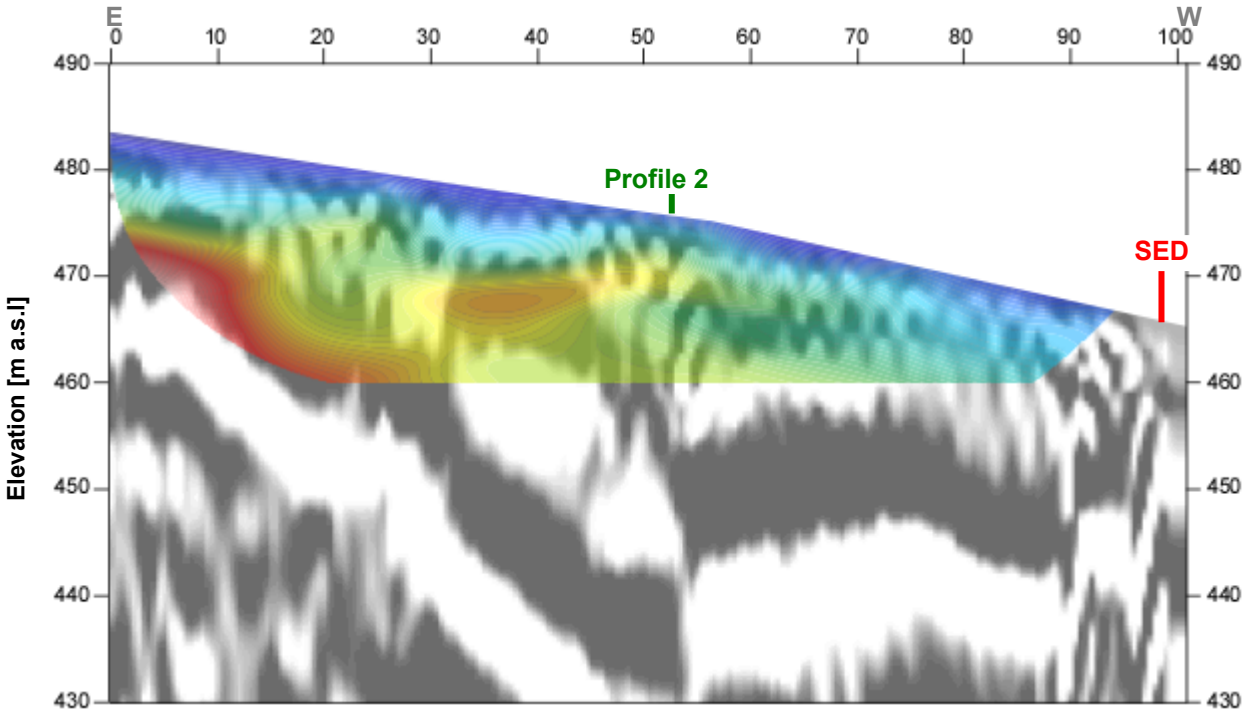

Fig. 3.4j Uninterpreted hybrid seismic section 09SN_01ACB-P1: superimposed onto the seismic reflection section is the color encoded p-velocity field derived by refraction tomography (no vertical exaggeration).

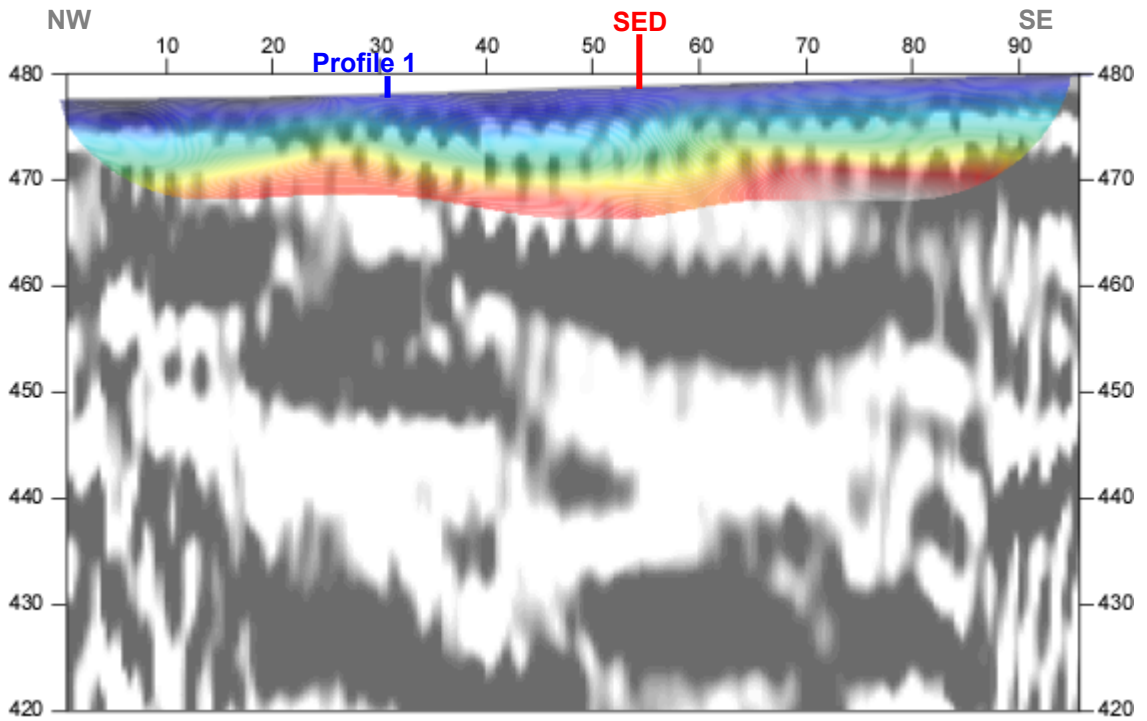

Fig. 3.4k Uninterpreted hybrid seismic section 09SN_01ACB-P2: superimposed onto the seismic reflection section is the color encoded p-velocity field derived by refraction tomography (no vertical exaggeration).

4 DISCUSSION OF THE RESULTS

4.1 Summary and Validation of the Results

Compressional and shear wave velocity data from refraction seismic surveys both p-wave and s-wave and also the MASW survey data from profiles 09SN_01ACB-1 and 09SN_01ACB-2 are shown in Tab. 4.1 for the uppermost 30 m. The calculated shear wave velocity $v_{s(calc)}$ in Tab. 4.1 is derived by using a theoretical v_p/v_s-ratio of $\sqrt{3}$.

Depth	Vp1	Vp2	Vs1	Vs2	Vs1	Vs2	Vs1	Vs2
	meas	meas	calc	calc	meas	meas	MASW	MASW
0	495	420	286	242	274	266		0
1	620	465	358	269	295	293	522	469
2	847	604	489	349	467	389	532	488
3	1129	694	652	401	702	418	532	484
4	1441	940	832	543	793	489		0
5	1729	1091	998	630	693	559	504	433
6	1939	1409	1119	813	559	630		0
7	2027	1575	1170	910	728	649	484	449
8	1949	1880	1125	1085	880	693		
9	1802	1999	1041	1154		862	552	
10	1763	2151	1018	1242		934		547
11	1812	2234	1046	1290		1078		
12	1895	2311	1094	1334			729	
13	1968		1136					
14			1166					687
15	2020		1190					
16	2061		1204				838	
17	2086		1209					843
18	2093		1202					
19	2083							
20							643	
21								
22								940
23								
24								
25								
26							1013	
27								
28								1131

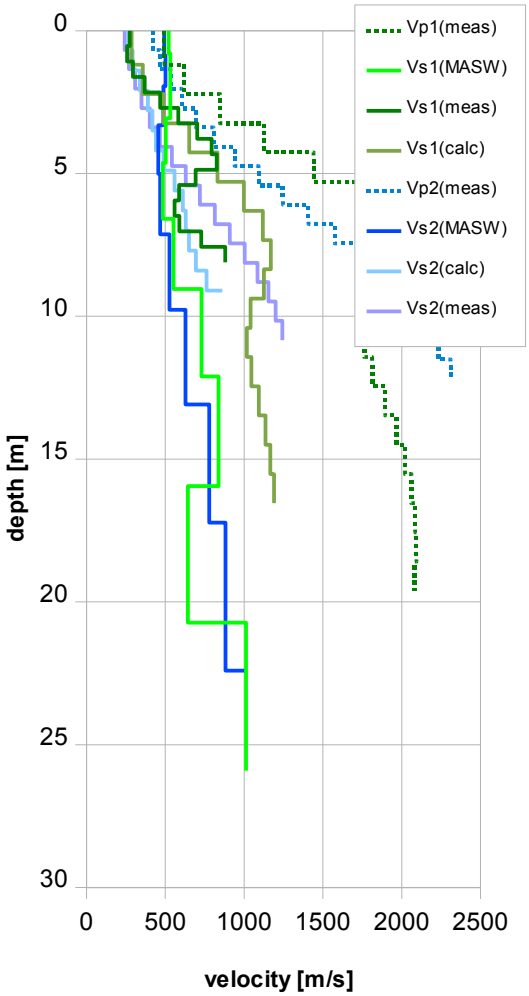

Tab. 4.1: Shear and compressional wave velocity model determined at the SED station ACB.

Fig. 4.1: Graphic display of shear (continuous lines) and compressional (dotted lines) wave velocities determined at the SED station. In green colors values from line 09SN_01ACB-1 and in blue values from line 09SN_01ACB-2. at the SED station.

4.2 Validation of the methods and their results

Due to methodological differences, v_s velocities derived by MASW analysis and by the refraction tomography technique may differ considerably. This is because MASW analysis cannot image small rock/soil inhomogeneities as a dispersion image with an array length of i.e. 40-m only yields one single v_s-value at each depth. On the other hand, refraction diving wave tomography results produce v_s-sections with a high lateral resolution, but fail to provide information at greater depths.

4.3 Error Estimates

The error estimates given in Tab. 4.3 below are relevant only in the context of this survey.

Surveying method	Type of result	Error estimate
v_s – refraction tomography	v_s – velocity field image	8%
MASW only "+" or only "-" values*	v_s – velocity field image	15%
MASW (mean of "+" & "-" values)*	v_s – velocity field image	10%
v_p – refraction tomography	v_p – velocity field image	5%
Reflection seismic surveying	Image of subsurface structures	n.a.

** MASW values in the uppermost 4 m are prone to an error of about 30 % (only one direction) resp. 20 % (mean of both directions.*

Tab. 4.3 Error estimates for the methods applied. Note that higher error estimates are to be taken into account with increasing depths.

The above error estimates are of a qualitative character only. In view of the intense fluctuations to be expected in both the lateral and vertical directions, any attempt to derive a quantitative general error estimate to be valid for the entire survey is to be considered as futile. In particular the topography variations on line 09SN_01ACB-1 have a certain impact on the quality of dispersion images. Nevertheless, all velocity data coincide well, independently from the methodological differences.

At the SED station ACB (Klingnau AG), the refraction velocity images both from shear and compressional wave analysis show coincident structures. The MASW figures are in the same range as the values obtained from the shear wave diving wave refraction tomography surveys.

4.4 The Geophysical Interpretation

The most conclusive information about the subsurface structures is provided by the results of the hybrid seismic section (v_p-refraction tomography profiling and reflection seismic section) and confirmed by the evaluation results of the v_s-refraction tomography data.

As can be seen from the v_s and v_p refraction tomography sections in Fig. 3.2e/f & Fig. 3.4g/h, the topography of the bedrock surface is imaged in detail on both profiles. The geological interpretation of the seismic events is shown in Fig. 4.2a. The rock surface seems to outcrop not far from the seismic profile 09SN_01ACB-1 in the west. To the east, the bedrock surface is situated at a depth of about 8 m. A clearly visible tectonic fault is imaged in the middle of the profile.

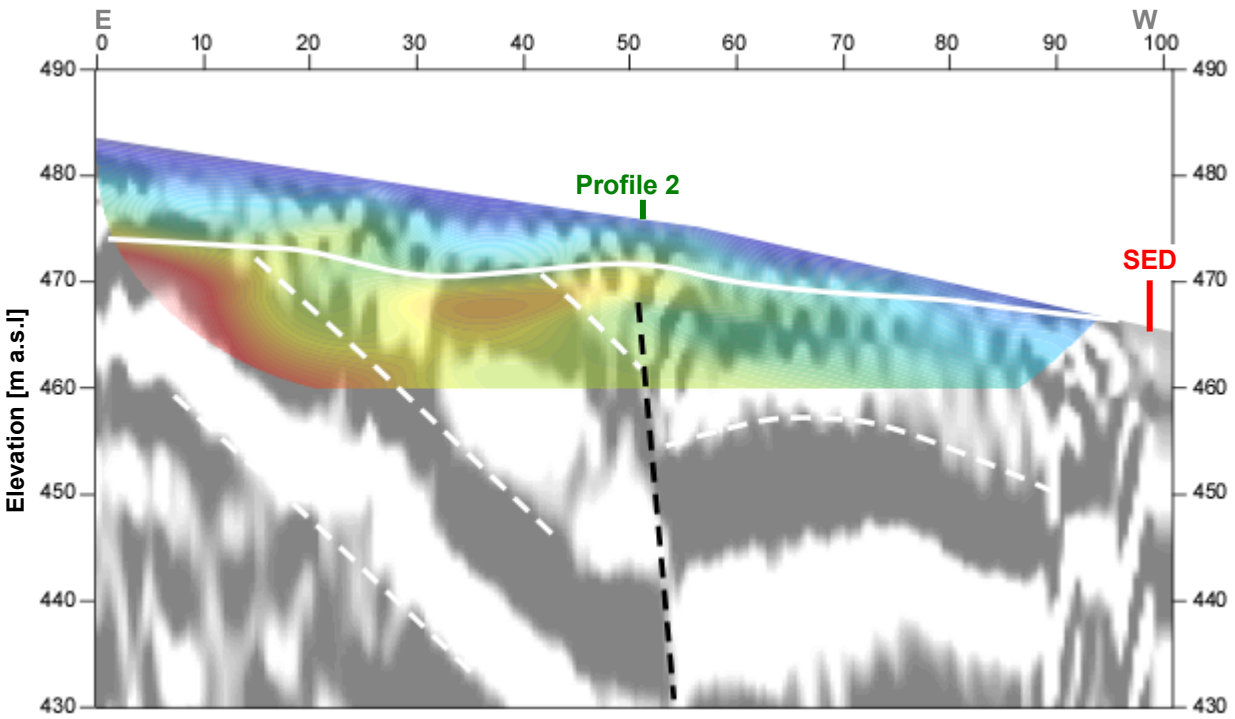

Fig. 4.2a Geophysical interpretation of the hybrid seismic section 09SN_01ACB-P1. White lines denote layer boundaries, continuous line the bedrock surface.

The geological interpretation of the seismic events of line 09SN_01ACB-2 is shown in Fig. 4.2a.Also on the second hybrid section 09SN_01ACB-2, the topography of the bedrock surface is imaged in detail all over the profile. The bedrock surface is imaged in a depth of about 5 to 8 m. As in profile 09SN_01ACB-1, the tectonic fault is visible near the intersection of the two seismic sections.

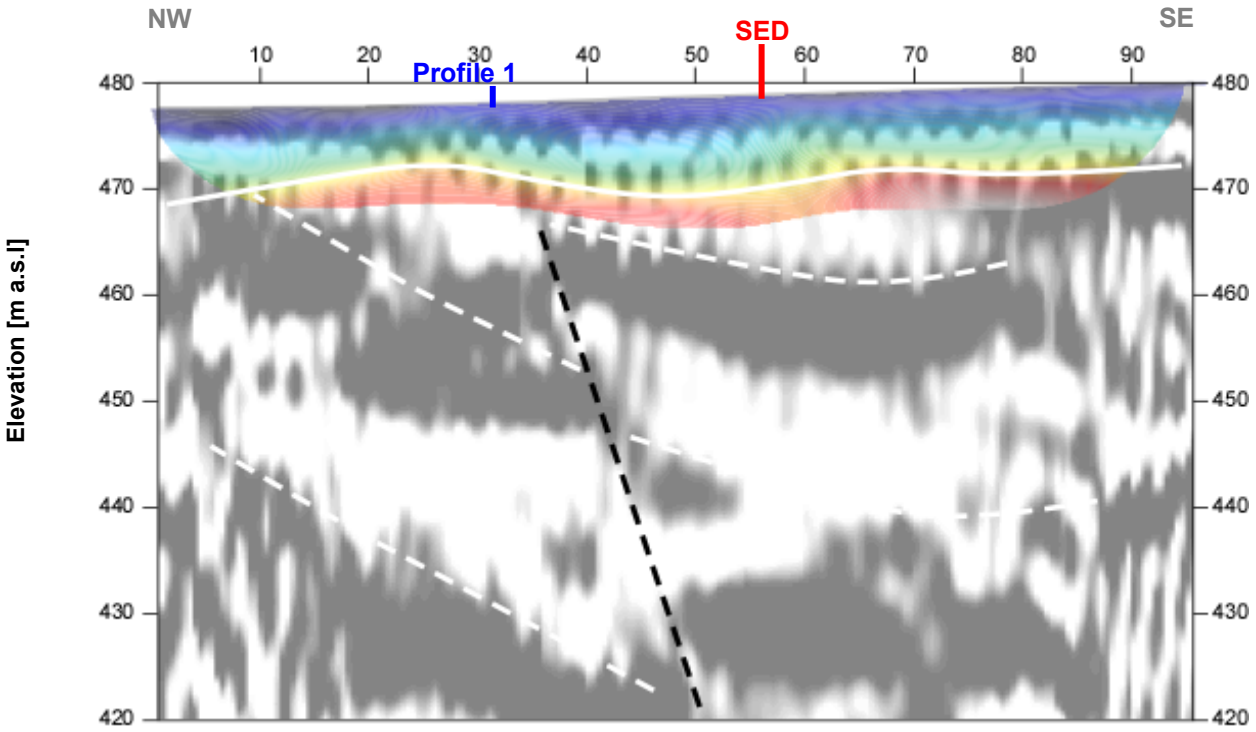

Fig. 4.2b Geophysical interpretation of the hybrid seismic section 09SN_01ACB-P2. White lines denote layer boundaries, the continuous one marks the bedrock surface; black dotted lines are indicative of suspected faulting with a wide loosening zone (black hatched area).

5 SUMMARY AND CONCLUSIONS

- In March 2009 a combined seismic s- and p-wave survey was carried out at the SED earthquake monitoring station near Klingnau AG.
- The shear wave data have been evaluated by conventional diving wave refraction tomography techniques in order to derive the s-wave velocity field along the seismic line. Due to the inherent constraints of the refraction tomography method, the depth of investigation is limited to 5 to 12 m under the prevailing geological conditions.
- The p-wave data have been processed
  - firstly to derive a 2D s-wave velocity field by using the MASW (**M**ultichannel **A**nalysis of **S**urface **W**aves) technique;
  - and secondly, according to the hybrid seismic data processing scheme for representing the subsurface structures in a combined reflection seismic section with the superimposed p-wave velocity field.
- The shear wave velocity range determined by the MASW method in the uppermost 30 meters spans from values of 433 m/s to 1131 m/s.
- The scalar values derived by the MASW survey at the SED station (seismic line 09SN_01ACB-M1, profile station 55; seismic line 09SN_01ACB-M2, profile station 45) are the following:

line 1			line 2		
$v_{s,5}$	=	530 m/s	$v_{s,5}$	=	487 m/s
$v_{s,10}$	=	516 m/s	$v_{s,10}$	=	478 m/s
$v_{s,20}$	=	615 m/s	$v_{s,20}$	=	556 m/s
$v_{s,30}$	=	634 m/s	$v_{s,30}$	=	631 m/s
$v_{s,40}$	=	n/a	$v_{s,40}$	=	n/a

- The maximum refraction shear wave velocity derived is 1078 m/s at a depth of 11 m.
- The maximum p-wave velocity determined is 2093 m/s at a depth of 18 m.
- The geophysical interpretation of the subsurface structures in this report are to be validated and incorporated into a comprehensive appraisal by a geologist familiar with the local geological setting.

Schwerzenbach, 5th May 2009

Walter Frei
dipl. Natw. ETH
managing director

Lorenz Keller
dipl. Natw. ETH
project manager